

AD-A246 428



NAVAL POSTGRADUATE SCHOOL Monterey, California



DTIC
SELECTE
FEB 28 1992
S B D

THESIS

Experimental Investigation of Energy
Dissipation in
Finite-Amplitude Standing Waves

by

LCDR Chen, Chih-Lyeu

June 1991

Thesis Advisor:
Co-Advisor

Anthony A. Atchley
Alan B. Coppens

Approved for public release; distribution is unlimited.

92 2 26 020

92-05005



Unclassified

Security Classification of this page

REPORT DOCUMENTATION PAGE			
1a Report Security Classification Unclassified		1b Restrictive Markings	
2a Security Classification Authority		3 Distribution Availability of Report	
2b Declassification/Downgrading Schedule		Approved for public release; distribution is unlimited.	
4 Performing Organization Report Number(s)		5 Monitoring Organization Report Number(s)	
6a Name of Performing Organization Naval Postgraduate School	6b Office Symbol (If Applicable) XX	7a Name of Monitoring Organization Naval Postgraduate School	
6c Address (city, state, and ZIP code) Monterey, CA 93943-5000		7b Address (city, state, and ZIP code) Monterey, CA 93943-5000	
8a Name of Funding/Sponsoring Organization	8b Office Symbol (If Applicable)	9 Procurement Instrument Identification Number	
8c Address (city, state, and ZIP code)		10 Source of Funding Numbers	
		Program Element Number	Project No Task No Work Unit Accession No
11 Title (Include Security Classification) EXPERIMENTAL INVESTIGATION OF ENERGY DISSIPATION IN FINITE-AMPLITUDE STANDING WAVES			
12 Personal Author(s) Chen, Chih-Lyeu			
13a Type of Report Master's Thesis	13b Time Covered From To	14 Date of Report (year, month, day) June 1991	15 Page Count 71
16 Supplementary Notation The views expressed in this thesis are those of the author and do not reflect the official policy or position of the Department of Defense or the U.S. Government.			
17 Cosati Codes Field Group Subgroup		18 Subject Terms (continue on reverse if necessary and identify by block number) finite-amplitude standing waves, quality factor, power input, dissipated power	
19 Abstract (continue on reverse if necessary and identify by block number) Thermoacoustic engines are designed to perform optimally at one frequency. However, the thermoacoustic prime movers have been shown to generate highly nonlinear waveforms, in which a significant amount of the acoustic energy appears in higher harmonics. This condition reduces the overall efficiency of the engine. The harmonics can be suppressed. But does the suppression mean that more energy remains in the fundamental frequency? This question is the topic of this thesis. Finite-amplitude standing waves were generated in a standing wave tube. The steady state input acoustic power was compared to the steady state dissipated acoustic power for two configurations - an empty tube and an obstructed tube - over a wide range of input powers. The waveforms in the empty tube were rich in harmonics, whereas the obstruction suppressed the harmonics significantly. The results of the measurements indicate that suppression of the harmonics also suppresses the transfer of energy from the fundamental.			
20 Distribution/Availability of Abstract <input checked="" type="checkbox"/> unclassified/unlimited <input type="checkbox"/> same as report <input type="checkbox"/> DTIC users		21 Abstract Security Classification Unclassified	
22a Name of Responsible Individual Anthony A. Atchley		22b Telephone (Include Area code) (408) 646-2848	22c Office Symbol PH/Ay

DD FORM 1473, 84 MAR

83 APR edition may be used until exhausted

All other editions are obsolete

security classification of this page

Unclassified

Approved for public release; distribution is unlimited.

EXPERIMENTAL INVESTIGATION OF ENERGY
DISSIPATION IN FINITE-AMPLITUDE STANDING WAVES

by

Chen, Chih-Lyeu
Lieutenant Commander, R.O.C. Taiwan Navy
B.S., Taiwan Provincial College of Marine and Oceanic Technology

Submitted in partial fulfillment of the requirements for
the degree of

MASTER OF SCIENCE IN ENGINEERING ACOUSTICS

from the

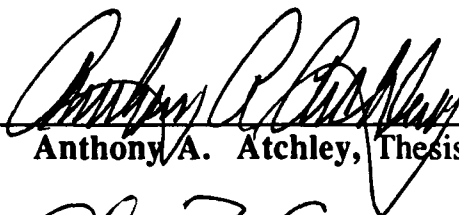
NAVAL POSTGRADUATE SCHOOL
June 1991

Author:



Chen, Chih-Lyeu

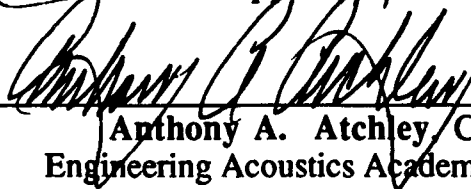
Approved by:



Anthony A. Atchley, Thesis Advisor



Alan B. Coppens, Thesis Co-Advisor



Anthony A. Atchley, Chairman
Engineering Acoustics Academic Committee

ABSTRACT

Thermoacoustic engines are designed to perform optimally at one frequency. However, the thermoacoustic prime movers have been shown to generate highly nonlinear waveforms, in which a significant amount of the acoustic energy appears in higher harmonics. This condition reduces the overall efficiency of the engine. The harmonics can be suppressed. But does the suppression mean that more energy remains in the fundamental frequency? This question is the topic of this thesis. Finite-amplitude standing waves were generated in a standing wave tube. The steady state input acoustic power was compared to the steady state dissipated acoustic power for two configurations - an empty tube and an obstructed tube - over a wide range of input powers. The waveforms in the empty tube were rich in harmonics, whereas the obstruction suppressed the harmonics significantly. The results of the measurements indicate that suppression of the harmonics also suppresses the transfer of energy from the fundamental.

Accession For	
NTIS CRA&I	<input checked="checked" type="checkbox"/>
DTIC TAB	<input type="checkbox"/>
Unannounced	<input type="checkbox"/>
Justification	
By	
Distribution/	
Availability Codes	
Dist	Avail and/or Special
A-1	

TABLE OF CONTENTS

I	INTRODUCTION	1
II	THEORY.....	4
	A. ENERGY CONSIDERATIONS.....	4
	1. Derivation of input power \dot{E} input.....	4
	2. Dissipated power \dot{E} for the empty tube	7
	B. SMALL-BUT-FINITE PERTURBATION THEORY CONSIDERATION	11
	C. OBSTRUCTED TUBE.....	13
	1. Resonance frequency of the obstructed tube.....	14
	2. \dot{E} of the obstructed tube	17
III	APPARATUS AND MEASUREMENTS.....	19
	A. EXPERIMENTAL SET-UP.....	19
	1. Resonant Tube	19
	2. Driver.....	21
	3. Accelerometer, microphone and calibration.....	22
	B. DATA ACQUISITION.....	23
IV	RESULTS AND DISCUSSION.....	27
	A. EMPTY TUBE	27
	1. Typical acceleration spectra, pressure spectra and waveforms...27	
	2. Q vs frequency	29
	3. Analysis of the input power and dissipated power.....	30
	B. OBSTRUCTED TUBE.....	38
	1. Typical acceleration spectra, pressure spectra and waveforms...45	
	2. Q versus frequency	46

3. Analysis of the input power and dissipated power.....	47
V. CONCLUSION.....	56
A. UNOBSTRUCTED TUBE.....	56
B. OBSTRUCTED TUBE.....	56
LIST OF REFERENCES	58
INITIAL DISTRIBUTION LIST.....	59

LIST OF TABLES

Table 1. Measured resonance frequency of the empty tube.....	35
Table 2. Measured resonance frequency of the obstructed tube.....	45

LIST OF FIGURES

Fig.	1. A plane-wave resonator of length $L = \lambda / 2$ and maximum values for $p(x)$, $u(x)$. The piston of driving the acoustic oscillation is not shown.	5
Fig.	2. Transmission and reflection of a plane wave inside an obstructed tube.....	15
Fig.	3. Schematic diagram of the experimental setup for generating finite-amplitude standing waves.	20
Fig.	4. The arrangement of the piston and the diaphragm. The curvature of the piston face is highly exaggerated.....	21
Fig.	5. Relative amplitude level of acceleration for fundamental and two overtones.....	22
Fig.	6. Side view of a pipe inside the tube.	26
Fig.	7. The spectrum and waveform observed at resonance of the fundamental of the tube for low piston Mach number case. (a) spectrum of acceleration. (b) spectrum of microphone output. (c) microphone output waveform.	31
Fig.	8. The spectrum and waveform for moderate piston Mach number case. (a) spectrum of acceleration. (b) spectrum of microphone output. (c) microphone output waveform.....	32
Fig.	9. The spectrum and waveform for high piston Mach number case. (a) spectrum of acceleration. (b) spectrum of microphone output. (c) microphone output waveform.....	33
Fig.	10. A typical least square fit of Q . Points represent the measured data; line is the ideal fit.....	34
Fig.	11. Experimental Q obtained from frequency response and energy method. Line is theoretical calculation from Eq. (19). \blacksquare represents the measured Q from energy method, \circ is the Q for frequency response.	35

Fig. 12.	Measured ratio of $\dot{E}/\dot{E}_{\text{input}}$. The ratio is plotted against the piston Mach number.....	37
Fig. 13.	Ratio of $\dot{E}_2+\dot{E}_3+\dots/\dot{E}_{\text{input}}$ for experimental data. The ratio is plotted against piston Mach number.....	39
Fig. 14.	Ratio of observed $\dot{E}/\dot{E}_{\text{input}}$ versus piston Mach number. Points are measured values. The experimental ratio has been compared to the ideal ratio of unity.	40
Fig. 15.	The comparison of observed harmonic amplitude and small-but-finite theory prediction, for three different piston Mach numbers.....	42
Fig. 16.	Ratio of resonance frequency with block inside the tube to the resonance frequency of empty tube. • represents the measured ratio, line is the theoretical calculation by using boundary conditions. Dashed line is the theoretical calculation from Rayleigh's theory..	44
Fig. 17.	The spectrum and waveform of the obstructed tube at low Mach number.	49
Fig. 18.	The spectrum and waveform of the obstructed tube at moderate Mach number.....	50
Fig. 19.	The spectrum and waveform of the obstructed tube at high Mach number.	51
Fig. 20.	Experimental Q of the obstructed tube (driven at two different piston Mach number) for the first five modes. Different symbols represent different Mach number: ◆, Mach number = 4.25×10^{-6} ; ▲, Mach number = 7.7×10^{-5} . The solid line is the theoretical Q.	52
Fig. 21.	Ratio of observed $\dot{E}/\dot{E}_{\text{input}}$ versus piston Mach number for the fundamental mode. Points are measured values. The experimental ratio has been compared to the ideal ratio of unity.....	53
Fig. 22.	Comparison of overall dissipation power by harmonics for unobstructed tube and obstructed tube. The abscissa is the acceleration amplitude in Mach number.....	54
Fig. 23.	Comparison of the fundamental component for empty tube and obstructed tube.....	55

ACKNOWLEDGMENTS

I am particularly grateful to my advisors, Professor Atchley and Professor Coppens for their guidance, support and encouragement in this work. I also wish to thank Dr. Gaitan without whom, quite literally, this thesis could not have been done. Next I thank George Jaksha of the Physics machine shop for his help in conducting the experiment.

Finally, I am most grateful to my wife, Chia-Huey, for her moral support and encouragement throughout my two years at the Naval Postgraduate School.

I. INTRODUCTION

Thermoacoustic engines, or acoustic heat engines, have been the subject of a number of scientific investigations over the past decade or so. One main reason for interest in thermoacoustic engines is the fact that thermoacoustic engines are energy-conversion devices that achieve simplicity by use of acoustic technology. One class of thermoacoustic engines consists of standing wave thermoacoustic engines, which are designed around an acoustic resonator. In these engines, the acoustic energy or power is generated by or supplied to the engine at the fundamental resonance frequency of the resonator. Standing wave thermoacoustic engines are designed to perform optimally at this frequency. Therefore, it is desirable that the acoustic energy remain in that fundamental mode. However, the acoustic pressure amplitudes involved are large enough for nonlinear effects to be important. Nonlinear effects will be manifested in the generation of harmonics of the fundamental frequency, thus taking energy out of the fundamental mode. Should nonlinear effects be important, a number of questions arise. How much of the input energy stays in the fundamental mode? How much energy is transferred to the harmonics? Is there a way to prevent this transfer?

Lin [Ref. 1] and Atchley, *et. al.* [Ref. 2] showed that the acoustic waveforms generated within a thermoacoustic prime mover can be highly nonlinear. In fact, the waveforms that they observed very closely resemble those generated by Coppens and Sanders [Ref. 3] in a geometrically simpler system ----- a rigid-walled standing wave tube. Coppens and Sanders studied

the problem of finite-amplitude standing waves and analyzed their results using a perturbation expansion solution of the nonlinear acoustic wave equation and taking into account viscous and thermal losses at the tube walls. The overall good agreement between their measurements and predictions showed that the standing wave tube is a good experimental apparatus for understanding finite-amplitude standing waves. Therefore, it was decided to try to find experimental answers to some of the questions raised above for the simple standing wave tube first, before using the more complex geometry of a thermoacoustic engine. These experimental investigations are the topic of this thesis.

The research was conducted in two phases ---- the empty tube phase and the obstructed tube phase. The empty tube phase served as a baseline, as a check of procedures and analysis techniques. The simplicity of the empty tube geometry makes analysis relatively straightforward. In this phase, the standing wave tube was driven at one end with a piston source, over a range of amplitudes from low up to those necessary for shock formation, at the fundamental frequency. Measurement of the steady state input acoustic power and the steady state acoustic power dissipated in each harmonic allowed determination of how much of the input energy stays in the fundamental mode and how much is transferred to the harmonics. These same measurements were repeated in the obstructed tube phase, which allowed the determination of whether or not there is a way to prevent the energy transfer.

The outline of this paper is as follows. In Section II, we describe the theory necessary to understand the concepts. The experimental setup and

procedures are described in Section III. Section IV is devoted to the discussion of the results. Finally, the conclusions are given in Section V.

II. THEORY

The goal of this thesis is to investigate experimentally the steady-state distribution of energy in finite-amplitude standing waves. In particular, it is desired to determine how the energy is transferred to harmonics due to nonlinear effects in the preshock regime. We shall begin this section, which is devoted to the basic energy considerations, by examining the total input power and the total dissipated power for the case of an empty tube. Next, we will consider the small-but-finite perturbation approach given by Coppens and Sanders. Finally, we will treat the more complicated situation, i.e., the obstructed tube.

A. ENERGY CONSIDERATIONS

1. Derivation of input power \dot{E}_{input}

Let us consider a closed, rigid, cylindrical tube of cross sectional area S (radius a), as shown in Fig. 1, with a length (along x) of L , and filled with air of density ρ_0 and sound speed c . The tube is rigidly terminated at $x = L$ and is driven by a piston at $x = 0$, not shown in the figure. The piston vibrates harmonically at the lowest resonance angular frequency ω of the resonator, so that $L = \lambda/2$. The air inside the tube oscillates longitudinally at angular frequency ω . If we take $x = 0$ at the left end of the tube, then the dependence of the acoustic pressure and velocity with distance for a plane wave in the tube is given by

$$p(x,t) = P_A \cos k(L-x) \sin \omega t, \quad (1)$$

$$u(x,t) = \frac{P_A}{\rho_0 c} \sin k(L-x) \cos \omega t. \quad (2)$$

where P_A is the pressure amplitude at the pressure antinodes of the standing wave, t is time and k is the wave number. Notice that under conditions of mechanical resonance for a rigid tube (at $x=0$ or $x=L$), $\sin k(L-x) = 0$, hence we have $kL = n\pi$.

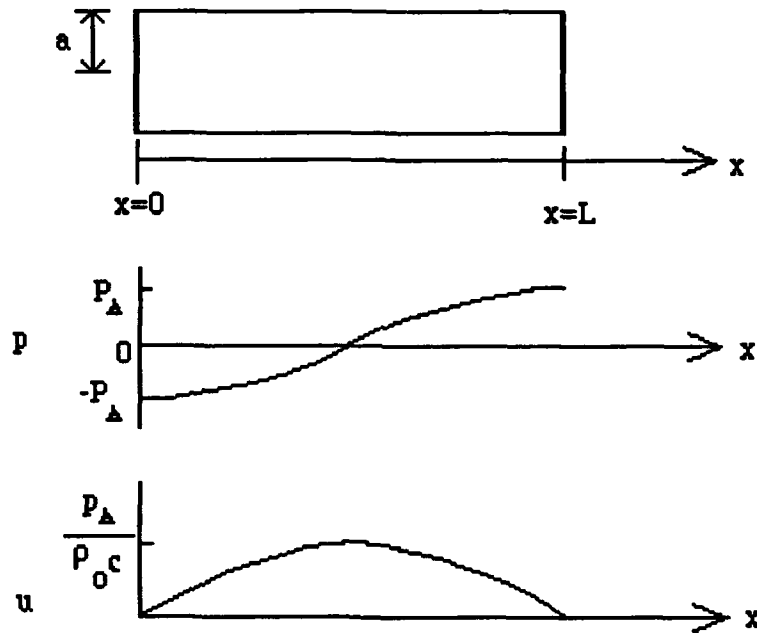


Fig. 1. A plane-wave resonator of length $L = \lambda / 2$ and maximum values for $p(x)$, $u(x)$. The piston of driving the acoustic oscillation is not shown.

The average rate of energy flow per unit area at a given location is equal to the mean value of the product of pressure and particle speed, thus

$$\text{acoustic intensity} = \frac{\text{acoustic power}}{\text{unit area}} = \langle p u \rangle, \quad (3)$$

where $\langle \cdot \rangle$ denotes a time average. We can represent the input power delivered by the piston as

$$\dot{E}_{\text{input}} = \langle u(0,t) p(0,t) \rangle S. \quad (4)$$

In Eq. (4), we have already explicitly used both pressure and velocity at the piston end. It can be shown [Ref 6: p206] that at resonance the pressure at $x=0$ and the velocity of the piston are in phase. The velocity of the piston can be represented in terms of the piston acceleration as

$$u(0,t) = \frac{A_0}{\omega} \sin(\omega t). \quad (5)$$

where A_0 is the peak acceleration amplitude of piston. Also, at resonance, the acoustic pressure at the piston can be written as

$$p(0,t) = P_A \sin \omega t. \quad (6)$$

Eq. (4) can then be rewritten as

$$\dot{E}_{\text{input}} = \left\langle \frac{A_0}{\omega} \sin(\omega t) \cdot P_A \sin(\omega t) \right\rangle S, \quad (7)$$

or carrying out the time average, Eq. (7) becomes

$$\dot{E}_{\text{input}} = \frac{P_A A_0}{2\omega} S. \quad (8)$$

Eq. (8) can be used to obtain the input power at resonance, if the pressure amplitude at the piston and the piston acceleration amplitude are known.

2. Dissipated power \dot{E} for the empty tube

Swift [Ref. 4] gives an elaborate discussion of the total dissipated power \dot{E} and the stored energy E_{st} for a plane-wave resonator. According to Swift the total dissipated power \dot{E} in a cylindrical tube of length L and radius R is

$$\dot{E} = \frac{1}{4} \frac{P_A^2}{\rho_0 c^2} \omega \pi R L \left[\delta_\kappa \left(\frac{\gamma-1}{1+\epsilon_s} \right) \left(1 + \frac{2R}{L} \right) + \delta_v \right]. \quad (9)$$

Here, ϵ_s is the ratio of the heat capacity of the gas to that of the tube wall, $\delta_v = \sqrt{2\nu/\omega}$ is the viscous penetration depth, with $\nu = \mu/\rho_0$ the kinematic viscosity and μ the dynamic viscosity. Also, $\delta_\kappa = \sqrt{2\kappa/\omega}$ is the thermal penetration depth, where $\kappa = k/\rho_0 c$ is the thermal diffusivity and k is the thermal conductivity. The reader is referred to Ref. 4 for a more complete discussion.

We will find it useful to express Eq. (9) in terms of the attenuation coefficient α . It is to be noted that, for steady state, the power delivered by the piston equals the power dissipated by the tube. Further, essentially all of the dissipated power \dot{E} arises from viscous and thermal effects at the tube walls.

In general, by using a microphone, we could determine the attenuation constant from

$$p_2 = p_1 e^{\alpha(x_2 - x_1)}, \quad (10)$$

where p_1 is the pressure amplitude at x_1 and p_2 that at x_2 (see Ref. 6: p208). This equation is applicable for traveling waves. We use standing waves. Hence, instead of determining α through Eq. (10), we determine it through the quality factor Q . The attenuation constant α can be determined by the quality factor Q_n of the n^{th} mode of the tube by $\alpha = \omega_n / 2Q_n c$. [Ref. 6: Eq. (30)] The quality factor Q , a measure of the sharpness of the frequency response of a driven resonator, may be measured or computed in several ways. One definition of Q is

$$Q = \omega \frac{E_{st}}{\dot{E}}, \quad (11)$$

where E_{st} is the energy stored in the resonator and \dot{E} is the power dissipated per cycle. To compute the Q from Eq. (11), we will need expressions for E_{st} and \dot{E} . We know that the energy transported by acoustic waves through a fluid medium is of two forms; the kinetic energy of the moving particles and the potential energy of the compressed fluid. The instantaneous energy density may be written as

$$\epsilon_i = \frac{1}{2} \rho_0 u^2 + \frac{1}{2} \frac{p^2}{\rho_0 c^2}. \quad (12)$$

The first term in Eq. (12) is the kinetic energy per unit volume; the second term is the compressive energy stored per unit volume. The time average of ϵ_i gives the time-averaged acoustic energy density ϵ at any point in the fluid, that is

$$\begin{aligned}\epsilon &= \langle \epsilon_i \rangle \\ &= \frac{1}{T} \int_0^T \frac{1}{2} \rho_o \left(u^2 + \frac{p^2}{\rho_o^2 c^2} \right) dt .\end{aligned}\tag{13}$$

Substituting Eqs. (1) and (2) into Eq. (13), we obtain simply

$$\begin{aligned}\epsilon &= \frac{1}{4} \frac{P_A^2}{\rho_o c^2} [\sin^2 k(L-x) + \cos^2 k(L-x)] \\ &= \frac{1}{4} \frac{P_A^2}{\rho_o c^2} .\end{aligned}\tag{14}$$

The total stored energy E_{st} is easily obtained by integrating the time-averaged acoustic energy density ϵ over the volume of the tube. This yields

$$E_{st} = \int \epsilon dv = \frac{1}{4} \frac{P_A^2}{\rho_o c^2} SL.\tag{15}$$

Once again, in steady state, the power dissipated by the tube is that delivered by the piston. Hence, the substitution of Eqs. (8) and (14) into Eq. (11) yields

$$Q = \omega \frac{\frac{1}{4} \frac{P_A^2}{\rho_0 c^2} SL}{\frac{P_A A_0}{2\omega} S} = \frac{1}{2} \frac{\omega^2 P_A L}{\rho_0 c^2 A_0} . \quad (16)$$

It is convenient to express the results of the preceding developments in terms of the rms (root-mean-square) amplitudes,

$$Q = \frac{\omega^2 P_{rms} L}{2\rho_0 c^2 A_{rms}} , \quad (17)$$

where P_{rms} and A_{rms} are the rms pressure and acceleration amplitudes, respectively.

Equation (16) is valid for an unobstructed tube with constant cross section. For the obstructed tube, we obtain the value of Q a different way, by measuring the frequency response. The Q value of the tube can then be determined by fitting the steady state frequency response to a standard resonance equation[Ref. 3: Eq. (1)]

$$V(\omega) = \frac{V_{max}}{\left[1 + \frac{\omega^2}{\omega_0^2} Q^2 \left(1 - \frac{\omega_0^2}{\omega^2} \right)^2 \right]^{\frac{1}{2}}} , \quad (18)$$

where ω is the angular frequency of the drive and ω_0 is the resonance angular frequency.

Returning to Swift's expression for \dot{E} , Eq. (9), substitution of Eqs. (9) and (15) into Eq. (11) gives

$$\frac{1}{Q} = \frac{\delta_v}{R} + \frac{\delta_k(\gamma-1)}{R(1+\epsilon_s)} + \frac{2\delta_k(\gamma-1)}{L(1+\epsilon_s)}. \quad (19)$$

Using Eq. (19), Eq. (9) can be expressed as

$$\begin{aligned} \dot{E} &= \frac{1}{4} \frac{P_A^2}{\rho_0 c^2} \frac{\omega \pi R^2 L}{Q} \\ &= \frac{1}{2} \frac{P_A^2}{\rho_0 c} \pi R^2 L \alpha. \end{aligned} \quad (20)$$

Eq. (20) expresses \dot{E} in terms of α .

B. SMALL-BUT-FINITE PERTURBATION THEORY CONSIDERATION

At steady state, the power input from the piston is equal to the total power dissipated by the tube, i.e.,

$$\dot{E}_{\text{input}} = \dot{E}_{\text{total}} \quad (21)$$

where

$$\dot{E}_{\text{total}} = \dot{E}_1 + \dot{E}_2 + \dot{E}_3 + \dots \quad (22)$$

The subscript "input" represents the energy input by the piston, while \dot{E}_1 , \dot{E}_2 , ... represent the power dissipated by the fundamental and higher harmonics, respectively. The question, "How is the input energy transferred to the harmonics?" now arises. That is, we want to know how much of the input

energy can be held in the fundamental and the overtones owing to the nonlinear mechanism.

To find the answer, we use the small-but-finite amplitude theory presented by Coppens and Sanders [Ref. 3]. Coppens *et. al.* give a detailed discussion of the subject. They use a perturbation technique to express a finite-amplitude standing wave as Fourier series in its harmonics. Also, they make several assumptions. They assume that the attenuation is small and the frequency is close to that of resonance.

From Coppens *et. al.*, when the amplitude of the piston is such that finite-amplitude effects are negligible, at the frequency of infinitesimal-amplitude resonance, the pressure at the rigid end of the tube can be approximated as

$$P_{11} \equiv \left(\frac{\rho_0 c A_0}{\omega} \right) [(\alpha L)^2 + \sin^2(kL)] , \quad (23)$$

where P_{11} is the first-order pressure amplitude.

When finite amplitude effects are taken into consideration, the pressure is modified by the presence of higher harmonics. That is

$$p(L,t) = P_1 \sin(\omega t) + P_2 \sin(2\omega t + \theta_2) + P_3 \sin(3\omega t + \theta_2 + \theta_3) + \dots \quad (24)$$

Again from Coppens *et. al.*, the approximations of pressure amplitudes of the first two harmonics are given by

$$P_{22} = \frac{P_{11}^2}{2} \left(\frac{\beta}{\rho_0 c^2} \right) Q_2$$

and

$$P_{33} = \frac{P_{11}^3}{2} \left(\frac{\beta}{\rho_0 c^2} \right)^2 Q_2 Q_3 \quad (25)$$

where Q_n are function of the parameter δ_n . The parameter δ_n can be expressed as a function of attenuation constant α . Recall that Coppens *et. al.* have already assumed that the attenuation is small and the driving frequency is close to that of resonance, so Eq. (23) - (25) are restricted to the experimental conditions that we have.

To evaluate Eq. (23) - (25) more accurately, we will, however, include more terms [Ref. 3 Eq. (34)]. Although they give more precise results, they are too awkward to be listed here.

Finally, we can use the full expressions for Eq. (23) - (25) to calculate \dot{E} and \dot{E}_{input} . Coppens *et. al.* have shown this approach to be reasonably accurate. Thus, we use it as a check of our procedures.

C. OBSTRUCTED TUBE

So far we have focused attention on the empty standing wave tube, in which the overtones are very nearly harmonic. We wish to investigate a standing wave tube for which this is not the case. The mode structure of a tube can be altered by inserting sections of pipe of smaller radius. The point of all of this is to see if the energy transfer from fundamental to higher harmonics can be altered or prevented by changing the mode structure of the tube. This section begins with discussion of the resonance frequency of an obstructed tube. Then, we discuss \dot{E} for the obstructed case.

1. Resonance frequency of the obstructed tube

Rayleigh [Ref. 5] gives a detailed discussion of the variable cross section tube. Basically, the idea is that the kinetic energy of the motion inside the tube must be equal to the potential energy. To make rapid progress, we summarize directly the result [Ref. 5: Eq. (7), p67]

$$\omega^2 = \frac{c^2 \pi^2}{L^2} \left\{ 1 - 2 \int_0^L \cos\left(\frac{2\pi x}{L}\right) \frac{\Delta S}{S} \frac{dx}{L} \right\}. \quad (26)$$

where ω is the resonance frequency and ΔS is the change of cross sectional area. We may apply Eq. (26) to the m^{th} harmonic, if we modify it by the substitution of $\cos(2m\pi x/L)$ for $\cos(2\pi x/L)$.

We can also use the concept of boundary conditions to evaluate the resonance frequency of an obstructed tube. In Fig. 2, we show the acoustic pressure inside the obstructed tube schematically. The waves propagating to the right can be expressed as follows:

$$p_A = A e^{j(\omega t - kx)}, \quad (27)$$

$$p_C = C e^{j(\omega t - kx)}, \quad (28)$$

$$p_E = E e^{j(\omega t - kx)}, \quad (29)$$

where A, C, and E are the complex pressure amplitudes for regions I, II and III, respectively. Also, we can write down equations for the waves propagating to the left as

$$p_B = B e^{j(\omega t + kx)}, \quad (30)$$

$$p_D = D e^{j(\omega t + kx)}, \quad (31)$$

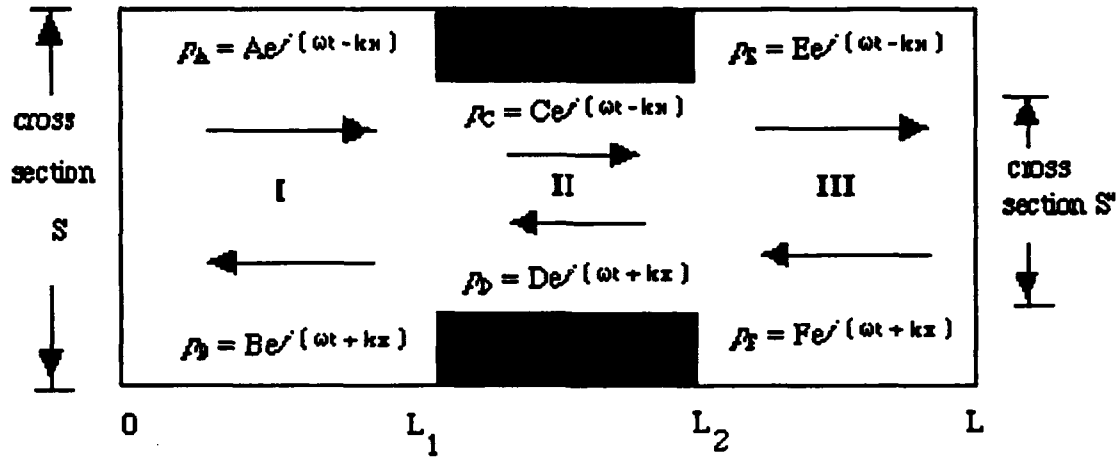


Fig. 2. Transmission and reflection of a plane wave inside an obstructed tube.

$$p_F = Fe^{j(\omega t + kx)}, \quad (32)$$

where B, D and F are the complex pressure amplitudes for regions I, II and III.

As usual, the boundary conditions are continuity of pressure and volume velocity at each point along the tube. Thus, we have six unknowns and six boundary conditions. The volume velocity U is the product of particle velocity u and cross sectional area S . It is to be noted that u can be expressed in terms of p as

$$u = \frac{p}{\rho_0 c} e^{j(\omega t \pm kL)}. \quad (33)$$

We begin at $x = L$, using Eqs. (29), (32) and Eq. (33), we obtain

$$U(L,t) = U_E(L,t) + U_F(L,t)$$

$$= \frac{S}{\rho_0 c} E e^{j(\omega t - kL)} - \frac{S}{\rho_0 c} F e^{j(\omega t - kL)} \quad (34)$$

$$= 0.$$

U_E represents the volume velocity due to p_E and U_F due to p_F . The pressure at $x = L$ can be written as

$$P(L,t) = E e^{j(\omega t - kL)} + F e^{j(\omega t + kL)} = P_L e^{j\omega t}. \quad (35)$$

From Eqs. (34) and (35), we find

$$E = \frac{1}{2} P_L e^{j k L} \quad (36)$$

and

$$F = \frac{1}{2} P_L e^{-j k L}. \quad (37)$$

Using similar procedure, we apply the boundary conditions at $x = L_2$, $x = L_1$ and $x = 0$ sequentially. We obtain expressions for A, B, C and D. After a long calculation and manipulation, we finally have the condition for resonance,

$$\begin{aligned} \sin(kL) - \left(\frac{1 - S/S'}{1 + S/S'} \right) \sin k(L - 2L_2) - \left(\frac{1 - S'/S}{1 + S'/S} \right) \sin(L - 2L_1) \\ + \left(\frac{1 - S/S'}{1 + S/S'} \right) \left(\frac{1 - S'/S}{1 + S'/S} \right) \sin[L - 2(L_2 - L_1)] = 0. \end{aligned} \quad (38)$$

This transcendental equation can be solved for the resonance frequency. The experimental results are compared with theoretical calculations for both Rayleigh's theory and boundary condition and shown in Section IV.

2. \dot{E} of the obstructed tube

Recall that for the case of the constant cross section tube, the total dissipated power \dot{E} is given by Eq. (9). Since the inner surface area of the tube changes after inserting the obstruction, we must perform the integration of the dissipation per unit area, \dot{e} [Ref. 4: Eq. (89)], over the different regions separately. The total dissipated power for the obstructed tube is, after a lengthy calculation and collecting the like terms,

$$\begin{aligned} \dot{E}_{\text{obstructed}} = & \frac{1}{4} \frac{P_A^2 \omega \pi R L}{\rho_0 c^2} \\ & \times \left[\delta_k (\gamma - 1) \left(1 - \chi + \frac{\sin k(1 - \chi)}{kL} + \frac{2R}{L} \right) + \delta_v \left(1 - \chi - \frac{\sin k(1 - \chi)}{kL} \right) \right] + \frac{1}{16} \frac{P_A^2 \omega \pi r L}{\rho_0 c^2} \left(1 + \frac{1}{r^2} \right)^2 \\ & \times \left[(1 + b^2 + 2b \cos \theta_1) (D_k + D_v) \right] \end{aligned} \quad (39)$$

where

$$r = \frac{\text{obstructed tube inner radius}}{\text{empty tube inner radius}},$$

$$\chi = \frac{\text{length of obstruction}}{\text{length of empty tube}},$$

$$b = \frac{1 - \left(\frac{1}{r}\right)^2}{1 + \left(\frac{1}{r}\right)^2},$$

$$\theta_1 = kL(1-\chi),$$

$$\Theta = \tan^{-1} \left(\frac{b \sin \theta_1}{1+b \cos \theta_1} \right),$$

$$D_k = \delta_k(\gamma-1) \left(\chi + \frac{\sin(kL(1+\chi) - \Theta)}{2kL} - \frac{\sin(kL(1-\chi) - \Theta)}{2kL} \right),$$

$$D_v = \delta_v \left(\chi - \frac{\sin(kL(1+\chi) - \Theta)}{2kL} + \frac{\sin(kL(1-\chi) - \Theta)}{2kL} \right).$$

Once $r, \chi, \delta_k, \delta_v$ have been determined, the \dot{E}_{input} is readily obtained from Eq. (39). To obtain the input power for the obstructed tube, we use the same equation as before, i.e., Eq. (8).

III. APPARATUS AND MEASUREMENTS

The first step toward accomplishing the goal of this thesis is to set up an apparatus which generates intense longitudinal standing waves within a rigid-walled tube. The set-up and use of the device is described in this section.

A. EXPERIMENTAL SET-UP

1. Resonant Tube

Figure 3 shows a diagram of the apparatus and instrumentation. The steel tube is 72.4 cm long, with a 5.72 cm inner diameter, and a wall thickness of 2.86 cm. One end of the tube is rigidly capped by a 2.48 cm thick aluminum cap and the other fitted with a piston. The tube contains air at ambient pressure and temperature. A microphone at the rigid end of the tube is used to measure the acoustic pressure as a function of time. An accelerometer is mounted on the piston to sense the piston's motion. The necessity of using a tube with very thick walls was indicated by previous research carried out by Coppens and Sanders [Ref. 3]. Coppens *et. al.* pointed out that an accelerometer mounted on the end of an aluminum tube with 0.32 cm wall thickness showed that the so-called "rigid" end cap actually vibrating with a significant amplitude. Because of this, we used the thick-walled tube which reduced the vibration of the tube. It is seen from Fig. 1 that the wavelength of the lowest mode of the standing wave is $\lambda = 2L$. Thus, the calculated resonance frequency of the lowest mode is about 236 Hz~238 Hz.

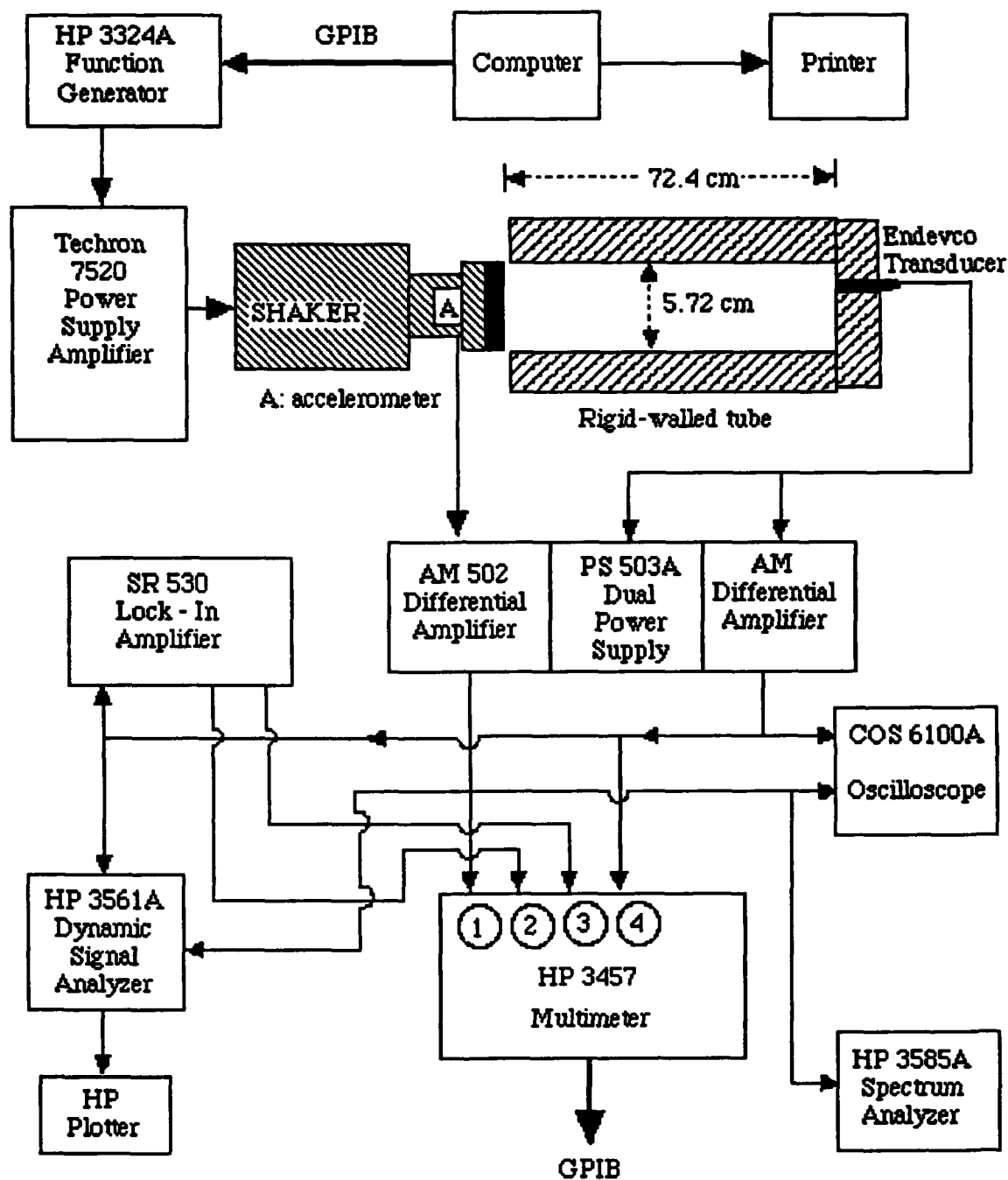


Fig. 3. Schematic diagram of the experimental setup for generating finite-amplitude standing waves.

2. Driver

The driver consists of a piston mounted on an MB Model EA 1500 PM shaker table. In operation, the piston surface contacts a thin diaphragm which seals the open end of the tube. The motion of the piston is monitored with an accelerometer. The arrangement is sketched in Fig. 4. The face of the piston was made with a very slight curvature so that there are no air pockets in between the piston face and the diaphragm, when the piston was aligned with the tube. We found that the diaphragm provided a better seal and less distortion of the piston motion than an O-ring seal. It is important that the motion of the piston be as free of harmonic distortion as possible.

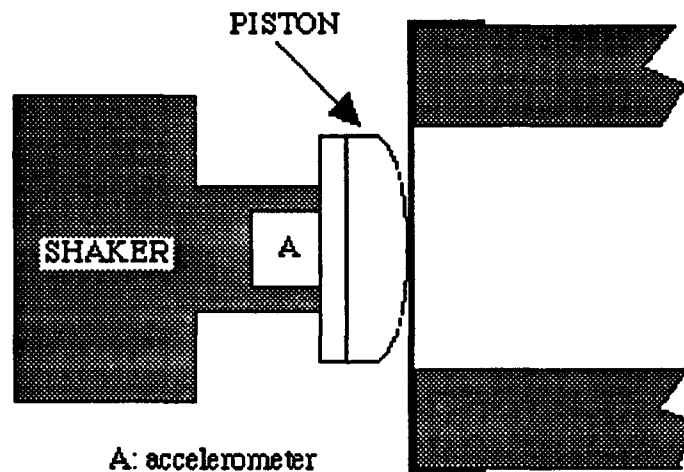


Fig. 4. The arrangement of the piston and the diaphragm. The curvature of the piston face is highly exaggerated.

The piston is very carefully aligned before measurements, so that the second- and third-harmonic distortions of the acceleration waveform were at

least 50 dB below the fundamental, i.e., 0.5% of the fundamental. Fig. 5 portrays the relative amplitude level for the fundamental and overtones of the acceleration.

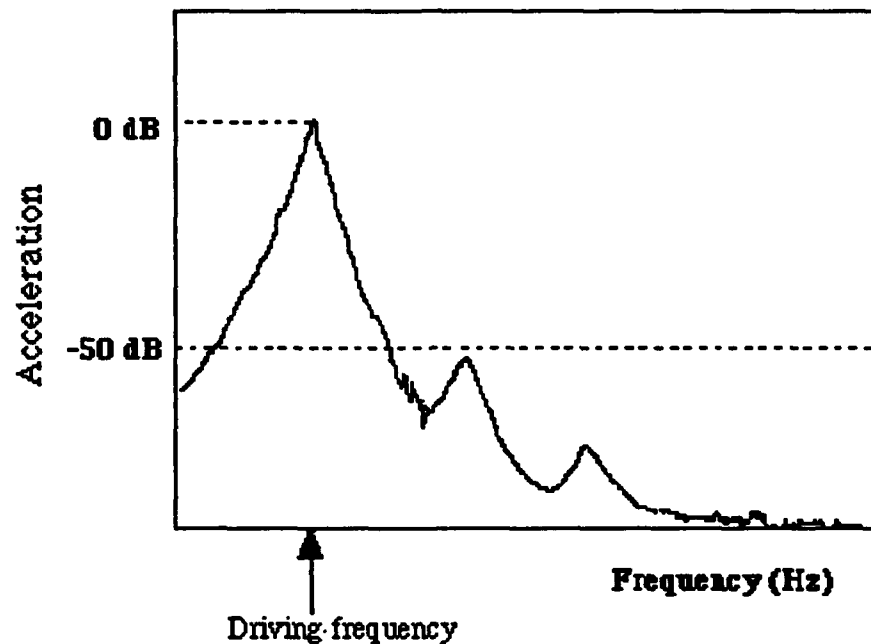


Fig. 5. Relative amplitude level of acceleration for fundamental and two overtones.

3. Accelerometer, microphone and calibration

As described above, an accelerometer is used to monitor the motion of the piston. We mounted an ENDEVCO accelerometer (serial number SN AJ31 type 2215) within the piston. The accelerometer output signal is amplified by TEKTRONIX AM Differential Amplifier with a gain of 100. A

tiny, 0.594 cm diameter, ENDEVCO Model 8510B-5 (serial number G63T) piezoresistive pressure transducer was mounted on the rigid end of the tube so that its diaphragm was flush with the end of the tube. The small diameter was chosen to minimize the disturbance of the rigid boundary condition. In general, the frequency response of the microphone was flat for the frequency range we were interested in. Its resonance frequency was greater than 50 kHz. Since the fundamental of the tube is around 238 Hz, this microphone was capable of faithfully reproducing the pressure waveform.

The experimental determination of the absorption coefficient α and the infinitesimal amplitude P_{11} requires absolute calibrations of both accelerometer and the microphone. We calibrated the accelerometer with a Brüel & Kjær calibration exciter (serial number 1343643). At frequency 159 Hz, ten determinations of the accelerometer sensitivity resulted in $S_A = 66.3 \pm 0.6$ mV/(m/s²). The sensitivity of the microphone was $S_M = 53.85$ mV/psi, according to manufacturer's specifications.

B. DATA ACQUISITION

The research was conducted in two phases: the empty tube phase and the obstructed tube phase. The same measurement sequences were performed in each phase. First, the Q was determined from Eq. (17) with the measured rms pressure and acceleration amplitudes at the resonance frequency. Next, the Q was determined by measuring the steady state frequency response and fitting the data to Eq. (18). Finally, the acceleration spectrum and the pressure spectrum and waveform were measured. These three sequences were repeated for various drive levels. Some specific details are given in this section.

As discussed in the previous section, to obtain the quality factor Q for the empty tube, we mainly used the energy method [Eq. (17)], but we still used the frequency response as a double check of procedures and analysis techniques during each data run.

In general, the measurement procedure was as follows:

First, we used the energy method to obtain the Q and the resonance frequency. The driving frequency was varied from below resonance (most of the time, the frequency resolution was set to 0.1 Hz), until the maximum microphone output was obtained. At this point, we recorded the values of P_{rms} and A_{rms} from the HP 3457 Multimeter, and then used Eq. (17) to obtain Q . To check for internal consistency, the run was immediately repeated by starting above the resonance and working down. It should be pointed out that we actually measured $p(L,t)$ rather than $p(0,t)$. However it can be shown that at resonance $p(L,t) = p(0,t)$.

Second, the measurement of Q using the frequency response method was accomplished by driving the resonator at frequencies near resonance of the lowest mode and measuring the steady state amplitude of the microphone output signal with the lock-in amplifier. Data acquisition was performed by a Standard 286 computer. Referring to Fig. 3, the computer communicates with the lock-in amplifier, the digital multimeter and the function generator through a GPIB interface. Through the execution of the controlling program, a source signal is supplied by the function generator to the piston. The accelerometer waveform was monitored by feeding the accelerometer output signal to differential amplifier (the gain is 100), the oscilloscope, and the HP 3585A spectrum analyzer. The output voltage from the microphone was

amplified by the second differential amplifier with a gain of 100 and sent to the lock-in. The output of the lock-in, as well as all other data signals of interest, were fed to the multimeter. The output of the multimeter is recorded by the computer. Also, the oscilloscope was used to monitor the output signal from the microphone. When data acquisition began, the approximate resonance frequency and the half-power bandwidth are entered into the computer, which then determines the start, stop frequencies and increment frequency. The program set the driving frequency and measured the output of the lock-in, then increased the frequency and repeated the process. After finishing the data acquisition, a least square fit is performed to obtain the resonance frequency and Q by using Eq. (18).

Third, once we determined the resonance frequency, we plotted the acceleration spectrum, microphone output spectrum and waveforms from the HP 3651A spectrum analyzer.

The procedures mentioned above were adopted for both empty tube phase and obstructed tube phase. For obstructed tube phase, we put concentric cylinders of different cross section in different positions inside the tube. To simplify our experiment, particular attention was paid to the case where the obstruction was in the middle of the tube. The reasons for this will be given in next section. The obstructions used in this experiment have the same wall thickness 0.634 cm with different length (10.2 cm and 5.2 cm). Fig. 6 shows the side view of a pipe inside the tube. The changes in resonance frequency and quality factor Q vary from one to another, but features are common. This will be discussed in more detail later. It is also to be noted that the values of resonance frequency obtained on consecutive runs differed by as much as 0.1

Hz. Because of the variation in room temperature, repeated measurements made at various times indicated that the value of the resonance frequency varied by as much as 0.3 Hz.

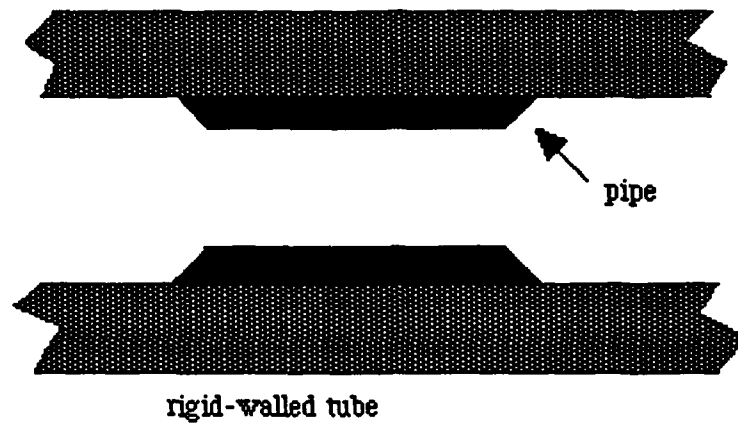


Fig. 6. Side view of a pipe inside the tube.

IV. RESULTS AND DISCUSSION

The results for both the empty and obstructed tube will be presented and discussed in this section. We begin by showing some typical features of pressure, acceleration spectra and waveforms. Secondly, we focus on the discussion of input power and dissipated power, and check the validity of our measurements by applying small-but-finite theory. Also, a comparison of the mode structure (resonance frequency harmonicity) for both cases will be given and discussed.

A. EMPTY TUBE

1. Typical acceleration spectra, pressure spectra and waveforms

The pressure and piston acceleration spectra and waveforms are represented in Fig. 7 - 9 for low, moderate, and high values of piston acceleration. In each case the tube is driven at its fundamental resonance frequency. The amplitudes in dBV of some of the spectral peaks are indicated in the figures. The conversion from dBV to pressure in Pa is calculated as follow:

$$P = (1280)(10^{\text{level in dBV}/20}) \text{ pa} ,$$

where we have used the microphone sensitivity of 53.85 mV/Psi and an amplifier gain of 100. Also the conversion from dBV to acceleration in m/s^2 is given as

$$\text{acc} = (15.08)(10^{\text{level in dBV}/20}) \frac{\text{m}}{\text{s}^2},$$

where we have used the accelerometer sensitivity 66.3 mV/m/s².

For the case of small acceleration amplitude (2.2 m/s²), the typical spectrum and waveform are shown in Fig. 7. As it can be seen from Fig. 7(b), the second harmonic is very small compared to the fundamental. The difference in spectrum level for the first two harmonics is larger than 35dB. That is, the second harmonic is 2% of the fundamental. Fig. 7(c) shows that the waveform is relatively sinusoidal and smooth. As the acceleration amplitude is increased, the waveform exhibits slight distortion, particularly in the negative portion of the cycle. Fig. 8 shows the corresponding spectrum and waveform when the acceleration amplitude is increased to about 24m/s². Notice that, from Fig. 8(c), the further steepening of the waveform has been enhanced by the growth of a secondary minimum in the latter part of the negative portion of the cycle. Inspection of Fig. 8(b) shows that, at this stage, the second harmonic has become 22% of the fundamental, and all of the higher harmonics have increased in value. This result shows that an increasing amount of the input energy is being transferred to higher modes. Now, as the acceleration amplitude is increased to above 30 m/s², the waveform is distorted even further and a strong shock appears. Fig. 9 shows the corresponding figures. It is important to note that, in Fig. 9(b), the difference between the first and the second harmonic has decreased further to less than 12dB. In other words, the second harmonic has become 25% of the fundamental. At this point, there is even more energy transferred to higher harmonics. A more common measure of the piston motion is the Mach

number of the piston rather than the acceleration. The Mach number is the ratio of the peak piston velocity divided by the speed of sound $u_0 / c = A_0 / \omega c$. The corresponding piston Mach numbers for Fig. 7, 8 and 9 are 4.3×10^{-6} , 5.8×10^{-5} , and 7.7×10^{-6} , respectively.

2. Q vs frequency

This experiment involves determining the resonance frequency and the quality factor by two different techniques: the energy method and frequency response. In Fig. 10, we show an example of the frequency response data, which is a graph of the amplitude of the microphone output as a function of driving frequency. The individual points represent the measured data, and the line represents the ideal response based on the fit to a standard resonance equation, Eq. (18).

The measured Q's for the first five modes are shown in Fig. 11. The piston Mach number is 4.3×10^{-6} . It is recalled that the Q of the tube is simply proportional to the ratio of R / δ , and furthermore, δ (either viscous or thermal) is proportional to $1 / \sqrt{\omega}$. Hence, Q should be proportional to $\sqrt{\omega}$. This is confirmed by the measurements. The figure indicates that the two measurement techniques are within a few percent. Also, the energy method gives slightly larger Q's than the frequency response. The theoretical Q is also plotted. It is calculated from Eq. (19). It is apparent that the measured Q's are consistently lower than the predicted ones. Although we can't explain this result, we do point out that it is consistent with results obtained by Coppens and Sanders [Ref. 3].

The measured resonance frequencies are shown in Table 1. Notice that the ratio of f_n / f_1 reveals the mode structure of the empty tube. It shows

the overtones are very nearly exact harmonics of the fundamental. Later, we will compare this ratio with that of the obstructed tube to get some insight.

3. Analysis of the input power and dissipated power

The input energy can be calculated from Eq. (4). Once again, when finite-amplitude effects are taken into consideration, the pressure is modified by the presence of higher harmonics. Thus, in order to evaluate the contribution from each component of $u(0,t)$ and $p(0,t)$, all we need is to express Eq. (4) in terms of their components. With these changes, the new expression for input power is shown as

$$\dot{E}_{\text{input}} = \langle (P_1 + P_2 + P_3 + \dots)(u_1 + u_2 + u_3 + \dots) \rangle S, \quad (40)$$

Since the time average of the cross terms, i.e., $p_1 u_2$, $p_1 u_3$, ..., will be zero, Eq. (40) can be simplified, with the substitution of Eq. (5) for each components of p and u , as follows:

$$\begin{aligned} \dot{E}_{\text{input}} &= \langle p_1 u_1 + p_2 u_2 + p_3 u_3 + \dots \rangle S \\ &= \left(\frac{p_1 A_1}{\omega_r} + \frac{p_2 A_2}{2\omega_r} + \frac{p_3 A_3}{3\omega_r} + \dots \right) S. \end{aligned} \quad (41)$$

where p_1, p_2, \dots are the peak values of the harmonics of the microphone output, A_1, A_2, \dots the peak values of the harmonics of the acceleration of the piston, and ω_r is the resonance frequency. The values of P_1, A_1 , etc were obtained from the spectra. \dot{E} is obtained from Eq. (20), using the measured Q .

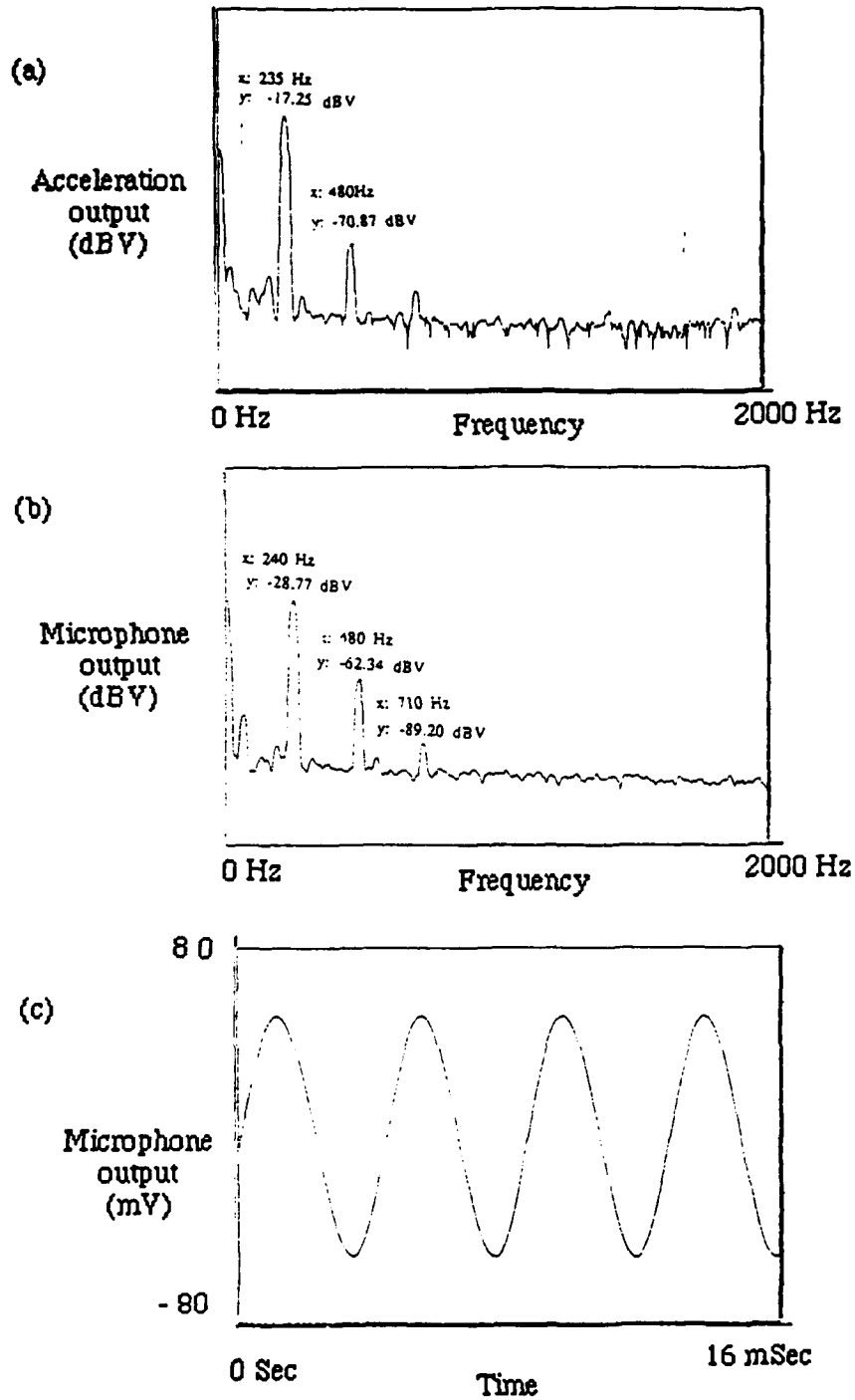


Fig. 7. The spectrum and waveform observed at resonance of the fundamental of the tube for low piston Mach number case. (a) spectrum of acceleration. (b) spectrum of microphone output. (c) microphone output waveform.

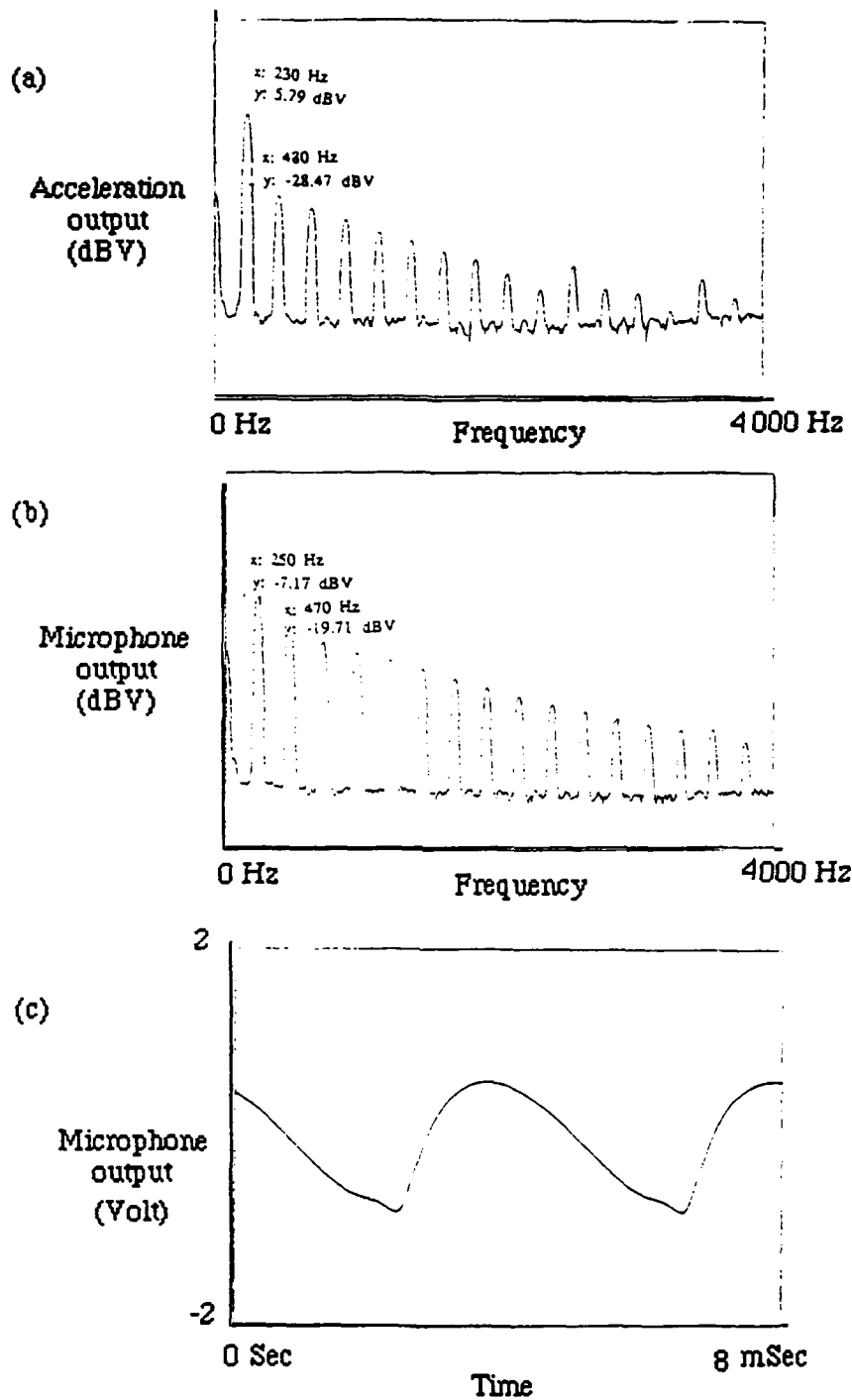


Fig. 8. The spectrum and waveform for moderate piston Mach number case. (a) Spectrum of acceleration. (b) spectrum of microphone output. (c) microphone output waveform.

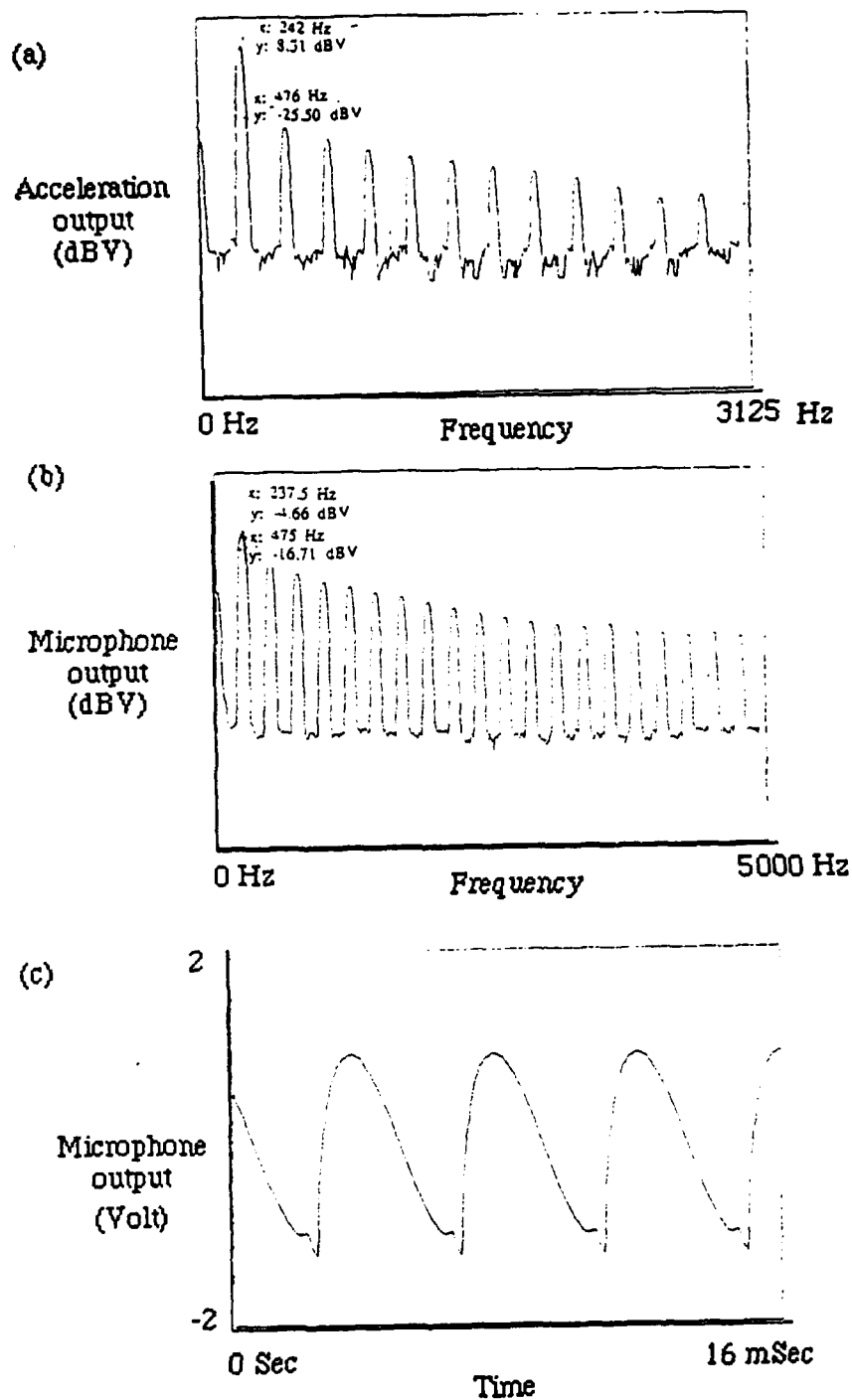


Fig. 9. The spectrum and waveform for high piston Mach number case.
 (a) spectrum of acceleration. (b) spectrum of microphone output.
 (c) microphone output waveform.

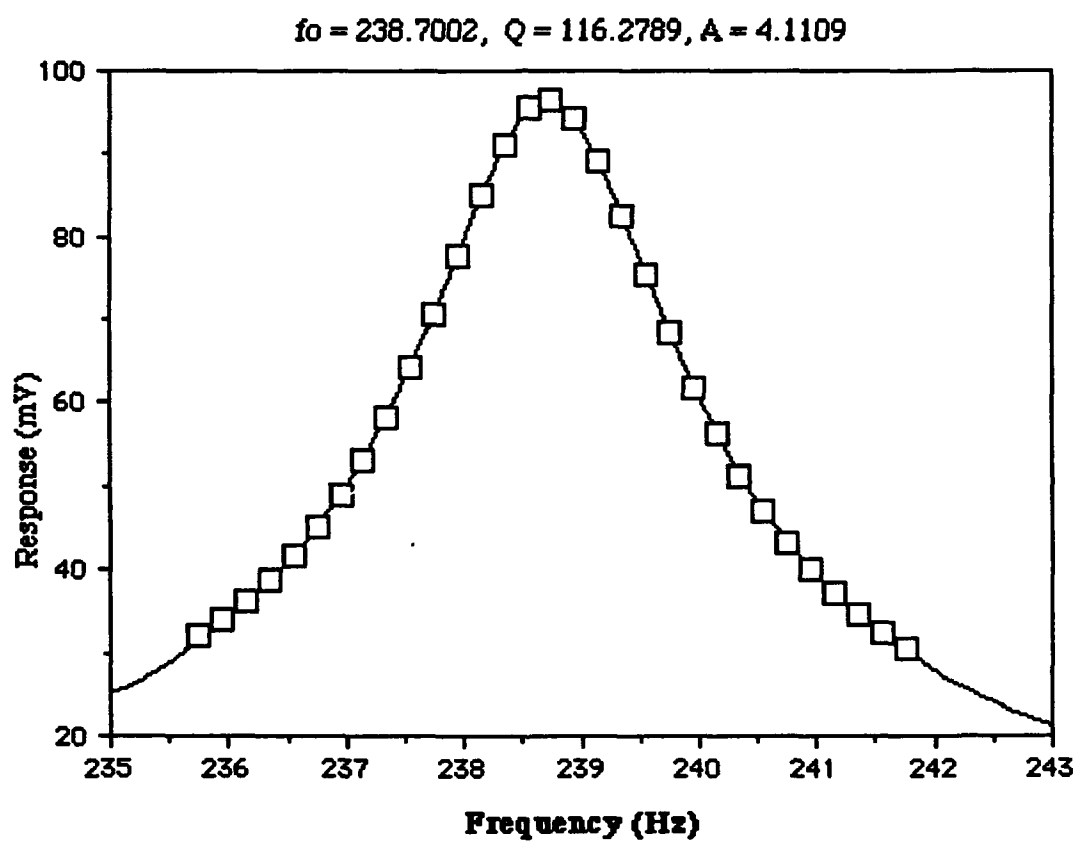


Fig. 10. A typical least square fit of Q . Points represent the measured data; line is the ideal fit.

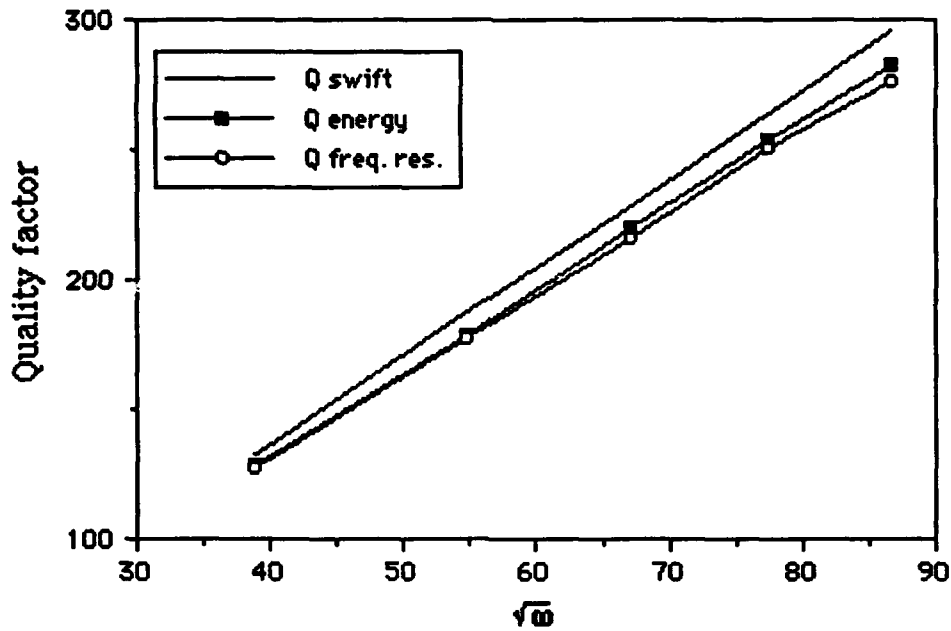


Fig. 11. Experimental Q obtained from frequency response and energy method. Line is theoretical calculation from Eq. (19). \blacksquare represents the measured Q from energy method, \circ is the Q for frequency response.

TABLE 1. MEASURED RESONANCE FREQUENCY OF THE EMPTY TUBE.

Mode	f_n	f_n / f_1
1	238	1.000
2	477	2.004
3	715	3.004
4	955	4.013
5	1194	5.017

The measurements were made by increasing the piston acceleration while the frequency was held at the fundamental mode of the tube. For the convenience of comparing the results, the values for total dissipation \dot{E} are grouped into two quantities, \dot{E}_1 and $\dot{E}_2 + \dot{E}_3 + \dots$, where $\dot{E}_2 + \dot{E}_3 + \dots$ represents the power dissipated by all of the harmonics except the fundamental. Also normalization has been used in presenting these results by using unitless fraction values. The results \dot{E}_1 are shown in Fig. 12. As the Mach number of the piston increases, the ratio of $\dot{E}_1 / \dot{E}_{\text{input}}$ decreases. The interpretation of this figure is that as more energy is put into the system, more energy is transferred to and dissipated by the harmonics generated by nonlinear mechanisms. In other words, the more energy we input, less of that input energy is stored in the fundamental. For example, in the low amplitude regime, almost all of the input power is stored in the fundamental, while for the high amplitude regime, only about 85% of that input power is held in the fundamental.

Fig. 13 shows the ratio of the energy dissipated by the higher harmonics, i.e., $\dot{E}_2 + \dot{E}_3 + \dots$ to the \dot{E}_{input} . It is also noted that the fifth and the higher harmonics are very small. Roughly speaking, the fifth harmonic amplitude is about 60 dB down with respect to the fundamental i.e., the fifth harmonic is only 0.1% of the fundamental, even for high acceleration amplitude. So, we only include the first five harmonics in the calculation of the total energy dissipation by all the overtones. It is sufficiently accurate for our purpose. Fig. 14 shows the ratio of total dissipated power to the input power. The individual points represent the experimental result, and the line is the ideal ratio of total acoustic dissipated energy to the total input energy, i.e., a ratio of 1. The maximum error is approximately 1%. Hence, Fig. 14

gives confidence that our techniques are valid and that all of the major sources of loss have been accounted for. However, there is a slight systematic decrease in the ratio at higher Mach number.

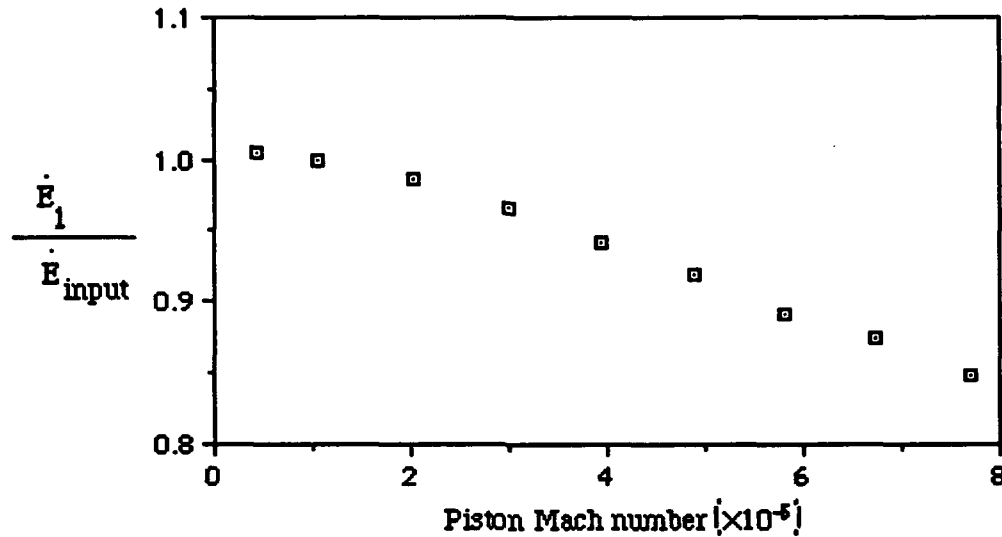


Fig. 12. Measured ratio of $\dot{E}_1 / \dot{E}_{input}$. The ratio is plotted against the piston Mach number.

Before we terminate our discussion of the empty tube, it is instructive to further investigate the validity of our measurements by comparing our results with the small-but-finite approximation theory proposed by Coppens *et. al.* [Ref. 3]. Fig. 15 shows the comparison between measured values and the theoretical prediction for different Mach number. From inspection of the figure, the following observations can be made: (1) for low Mach numbers (roughly speaking, acceleration amplitudes is below 1×10^{-5}), the agreement between the theoretically predicted values from small-

but-finite theory and measurements is qualitatively and quantitatively good for the first few components (Fig. 15(a) only shows the comparison for the first three components P_{11} , P_{22} , P_{33}). (2) When the Mach number is raised up to about 3.0×10^{-5} , the comparison indicates that the theoretical P_{11} and P_{33} are slightly larger than the measured results. The results suggests that the small-but-finite theory fails to provide sufficient convergence for the leading terms to adequately represent the harmonic distortion (Fig. 15(b)). (3) Finally, we see from the comparison of Fig. 15(c) that, for high enough Mach number (about 6.72×10^{-5}), theoretical values for P_{33} , P_{44} , P_{55} ... grow to more pronounced values than those of P_{11} and P_{22} .

B. OBSTRUCTED TUBE

The measurements on the empty tube indicate that as much as 15% of the input energy is lost from the fundamental. The question to be answered now is "Is there a way to prevent this transfer?" The transfer of energy is most efficient when the overtones of the resonator are exactly harmonically related to the fundamental resonance frequency. The empty tube closely matches this condition as indicated in Table 1. One method of preventing the transfer of energy is to alter the mode structure of the tube so that the overtones are no longer harmonic of the fundamental. This is the purpose of the obstruction. Extensive experiments were made by using a number of different obstructions, located at different positions along the tube, to find which gives the most significant effects. Inspection of our work reveals that the pipe of length 5.2 cm is the best choice for our purpose. Hence, from now on we only show the experimental data for this pipe, but the common features are still applicable to other obstructions.

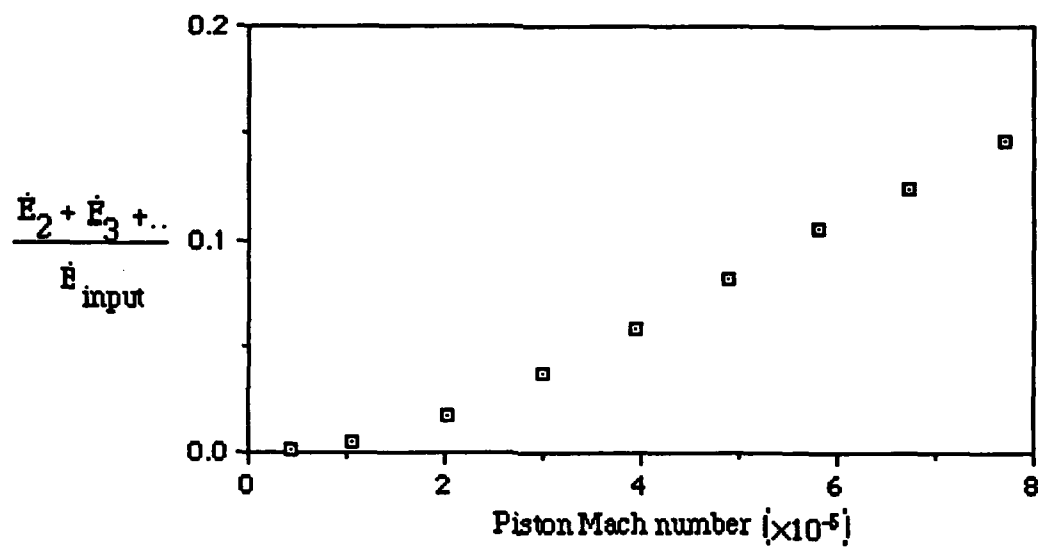


Fig. 13. Ratio of $\dot{E}_2 + \dot{E}_3 + \dots / \dot{E}_{\text{input}}$ for experimental data. The ratio is plotted against piston Mach number.

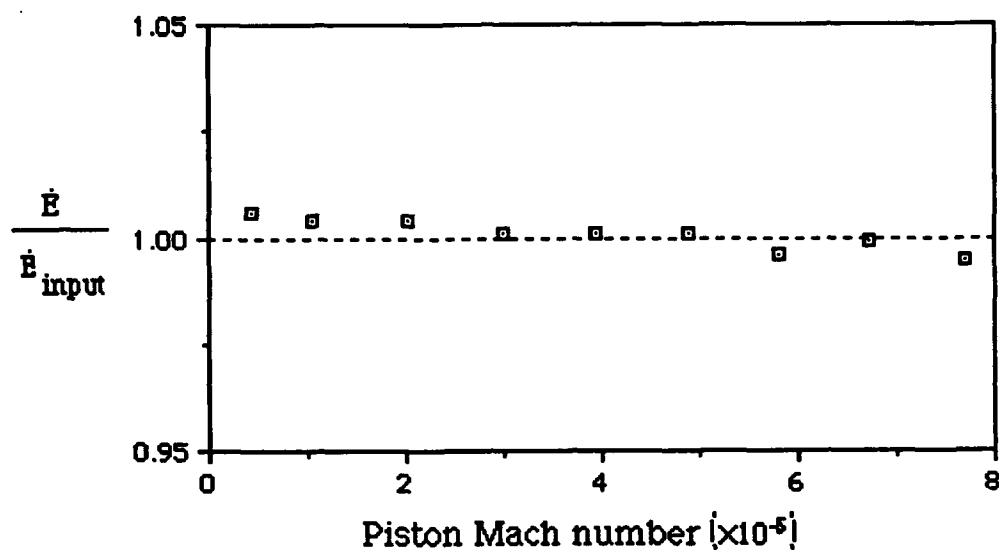
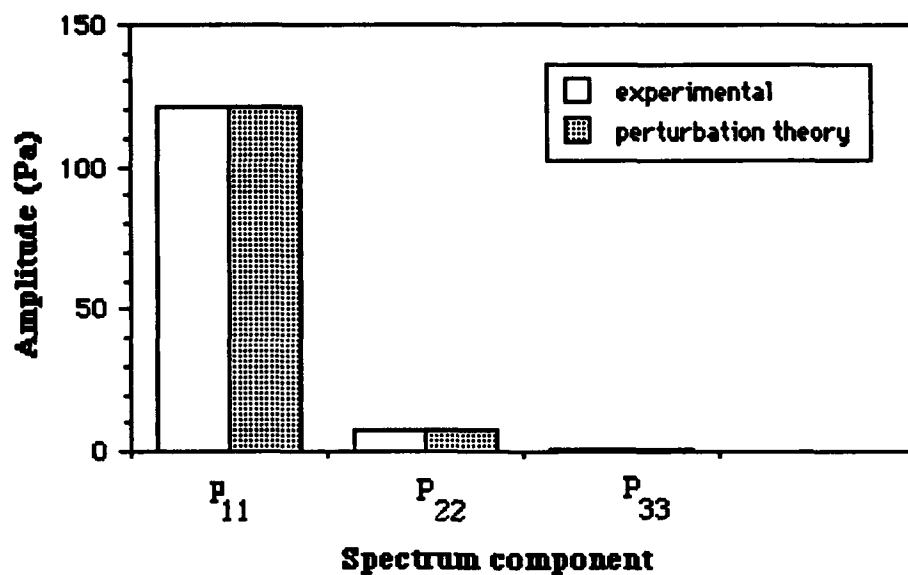
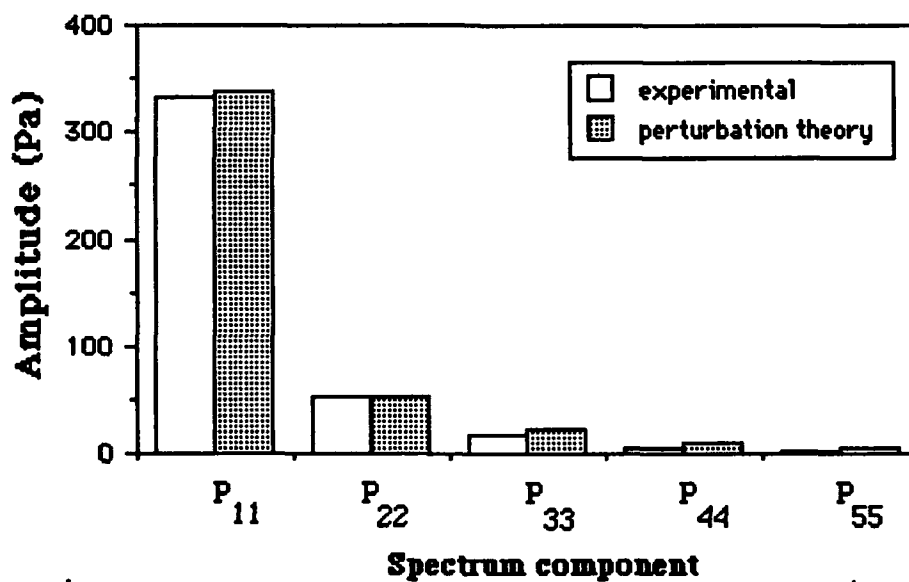


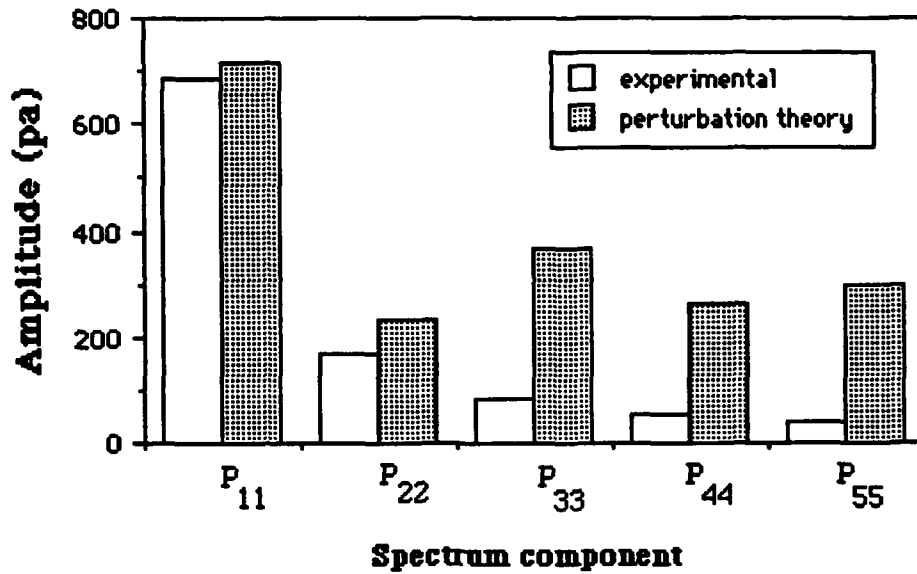
Fig. 14. Ratio of observed $\dot{E} / \dot{E}_{input}$ versus piston Mach number. Points are measured values. The experimental ratio has been compared to the ideal ratio of unity.



(a) Low piston Mach number (1.05×10^{-5})



(b) moderate piston Mach number (2.99×10^{-5})



(c) Strong piston Mach number (6.72×10^{-5})

Fig. 15. The comparison of observed harmonic amplitude and small-but-finite theory prediction, for three different piston Mach numbers.

To examine the resonance frequency change, comparisons of the experimental results and theory as a function of block position inside the tube are shown in Fig. 16.

In Fig. 16, the abscissa represents the position of the pipe center. We measure the pipe center position from the rigid end cap face. As can be seen from Eq. (25), the sound speed c will affect the calculated resonance frequency due to the uncertainty in the temperature. To get rid of this uncertainty introduced from the sound speed c , we use ratios rather than the absolute resonance frequencies. Thus, the ordinate is the unitless ratio of resonance frequency of the obstructed tube to the resonance frequency of the empty tube.

The dashed line represents the theoretical ratio from Rayleigh's theory [Eq. 26]. The solid line represents the calculation made by matching the boundary conditions. The individual points represent the experimental ratios. As revealed in Fig. 16, the ratio is greater than one when the pipe is near both ends. When the pipe is in the middle of the tube, the ratio reaches its minimum. From inspection of this figure the following observation can be made:

- The effect of a variation in cross section is greater near a pressure node or near pressure antinodes.
- At the points midway between the nodes and antinodes a slight variation of section is without effect.

The agreement between measurements and calculations from boundary conditions is surprisingly good. The discrepancies maybe due to the gap in between the tube wall and the pipe. Although we used a thick layer of vacuum grease, there may still be cavities formed after we slide the pipe into the middle of tube. One advantage of using a pipe is that the radial symmetry of the pipe will simplify the mathematical derivation of power dissipation \dot{E} for the obstructed tube case. Moreover, putting the pipe in the middle allows us to visualize more easily the standing wave in the obstructed tube from a longitudinally symmetric point of view. Hence, this suggests the middle position should be used to perform our experiment. Furthermore, we show the measured frequencies and the theoretical resonance frequencies of the obstructed tube in Table 2. Inspection of Table 1 and Table 2 reveals that the mode structure of the tube has been changed dramatically by the obstruction. Especially, the ratios of the second- and fourth modes are changed more, compared to those of empty tube. The point of all of this is that the

obstruction can change the mode structure. Thus, we might use some kind of obstruction to prevent the energy transfer from the fundamental to higher harmonics.

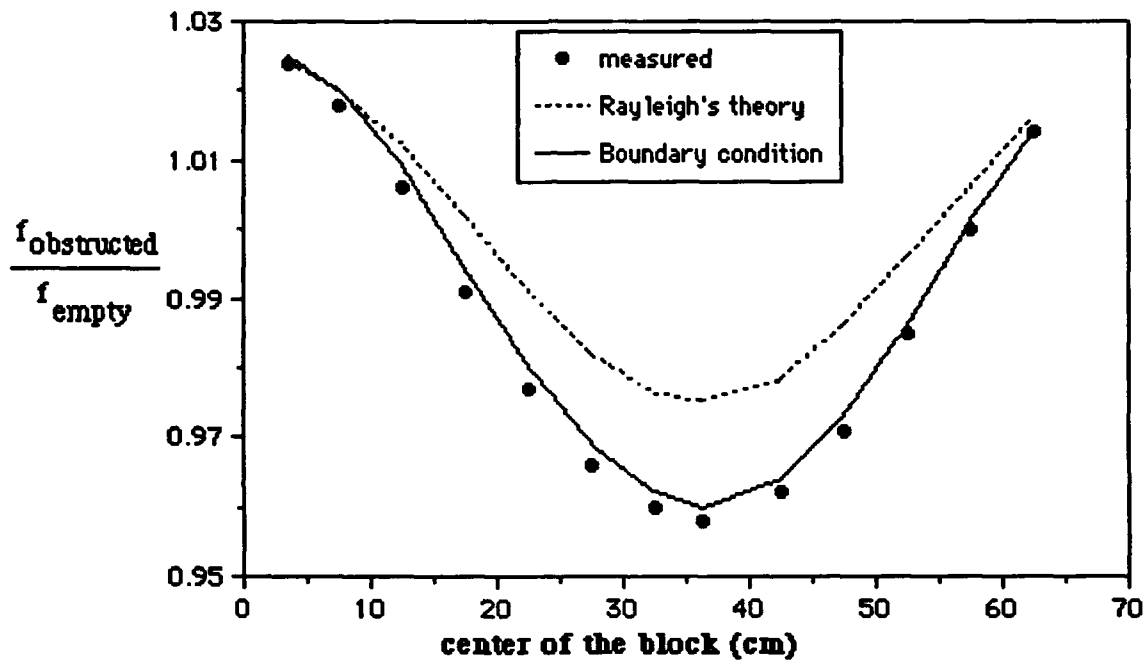


Fig. 16. Ratio of resonance frequency with block inside the tube to the resonance frequency of empty tube. • represents the measured ratio, line is the theoretical calculation by using boundary conditions. Dashed line is the theoretical calculation from Rayleigh's theory.

TABLE 2. MEASURED RESONANCE FREQUENCY OF THE OBSTRUCTED TUBE

Mode	f_n	f_n / f_1
1	227	1.000
2	487	2.144
3	686	3.019
4	974	4.289
5	1153	5.077

1. Typical acceleration spectra, pressure spectra and waveforms

Fig. 17 shows the corresponding spectra and waveforms for low piston Mach number in the stepped tube (the Mach number is 4.26×10^{-6}). From Fig. 17(a) and (b), we can see that the spectrum level difference between the fundamental and the second harmonic is about 60 dB, i.e., the second harmonic is about 0.1% of the fundamental. Fig. 17(c) shows the microphone waveform is sinusoidal. We see from the comparison of Fig. 7 and Fig. 17 that both cases have the same Mach number and both output displays are similar with the only difference being that the second harmonic of the obstructed tube is about 12% that of unobstructed tube. For moderate Mach number, the corresponding spectrum and waveform are shown in Fig. 18. Only the first three or four harmonics are big enough to be measured. Inspection of Fig. 8 and Fig. 18 reveals that the obstructed tube suppresses the higher harmonics. Finally, when the Mach number is even increased to 7.7×10^{-5} (which is much higher than the case of Fig. 9), the microphone output is

sinusoidal and there is no shock in the waveform. Fig. 19 shows the spectrum and waveform for the high acceleration amplitude case. From inspection of Fig. 9 and Fig. 19, the following observations can be made.

- The microphone output only has three or four harmonics. This is a big difference compared to the result of the unobstructed tube.
- The waveform is almost purely sinusoidal (Fig. 19(c)). On the other hand, the waveform of the unobstructed tube is highly distorted, as shown in Fig. 9(c).

This comparison remarkably demonstrates that the obstruction inside the rigid-walled tube significantly suppresses the higher harmonics. Subsequently, we can draw a conclusion which will be important for further research in thermoacoustic engines: obstructions can prevent the input power from being transferred from the fundamental to higher harmonics.

2. Q versus frequency

In Fig. 20, we show the frequency dependence of Q for the five modes. The Q's were obtained from the frequency response. In general, the Q values for different amplitudes do not coincide, but the common trend of Q is proportional to $\sqrt{\omega}$. From the inspection of Table 1 and Table 2, we can see the resonance frequency of the second and fourth modes are shifted upward. For example, for the second mode, the resonance frequency is shifted from 477 Hz up to 487 Hz. On the other hand, the resonance frequency of the first, third, and fifth modes are shifted downward. As a second example, for the third mode, the resonance frequency is shifted from 715 Hz for empty tube down to 686 Hz for the obstructed tube. Q's of the obstructed tube were measured to be less than expected from classical damping, probably due to excess attenuation generated in the gap between the obstruction and the tube.

3. Analysis of the input power and dissipated power

As mentioned earlier in section II, to compute the total dissipated power \dot{E} for the obstructed tube, we use the expression described by Eq. (28). The calculation of input power is the same for both the obstructed and unobstructed cases. Also, as before, we represent the results by using the ratio of total dissipated power \dot{E} to the total input power \dot{E}_{input} . We plot the typical ratio $\dot{E}/\dot{E}_{\text{input}}$ for the fundamental mode against the acceleration amplitude in Fig. 21. It is to be emphasized that \dot{E} includes only the fundamental of the microphone output spectrum. As noted earlier (Figs. 17-19), for the obstructed tube, the second harmonic is very small and there are only a few harmonics in the microphone output spectrum. Moreover, inspection of those data reveals that the second harmonic are always 35 dB down with respect to the fundamental, i.e., the second harmonic is less than 2% of the fundamental. Therefore, we calculate \dot{E}_{total} using \dot{E}_1 only. On the other hand, we do not show the ratio $\dot{E}_2 + \dot{E}_3 + \dot{E}_4 + \dots$ because the power dissipated by higher harmonics is small enough to be ignored. Figure 21 shows the ratio $\dot{E}/\dot{E}_{\text{input}}$ versus piston Mach number. The results indicate that not all of the energy is accounted for. There is a gradual decrease in the ratio of energies. The reasons for this decrease are not understood. Possible reasons are excess attenuation due to unavoidable cavities between the tube and obstruction or turbulence at the boundary of the obstruction. This topic needs further investigation.

Before we terminate our discussion, it is instructive for us to compare the spectral components of the microphone output for unobstructed and obstructed tube (see Fig. 22). It is clear from Fig. 22 (a) that the slope of the

line representing the fundamental decreases with increasing Mach number. In Fig. 22(b), we see the slope is almost constant over the whole range of acceleration. Also, it can be seen the second harmonic is quite small compared to that of unobstructed tube. Fig. 23 shows the fundamental component of the microphone output for both empty and obstructed cases. It can be seen, over the low amplitude range (below 5×10^{-5}), the microphone output of both cases are almost the same. At higher acceleration amplitudes, the pressure amplitude in the empty tube is less than in the obstructed tube. The difference is about 7% at the highest Mach number. Once again, the figure indicates that suppression of the harmonics also suppresses the transfer of energy from the fundamental.

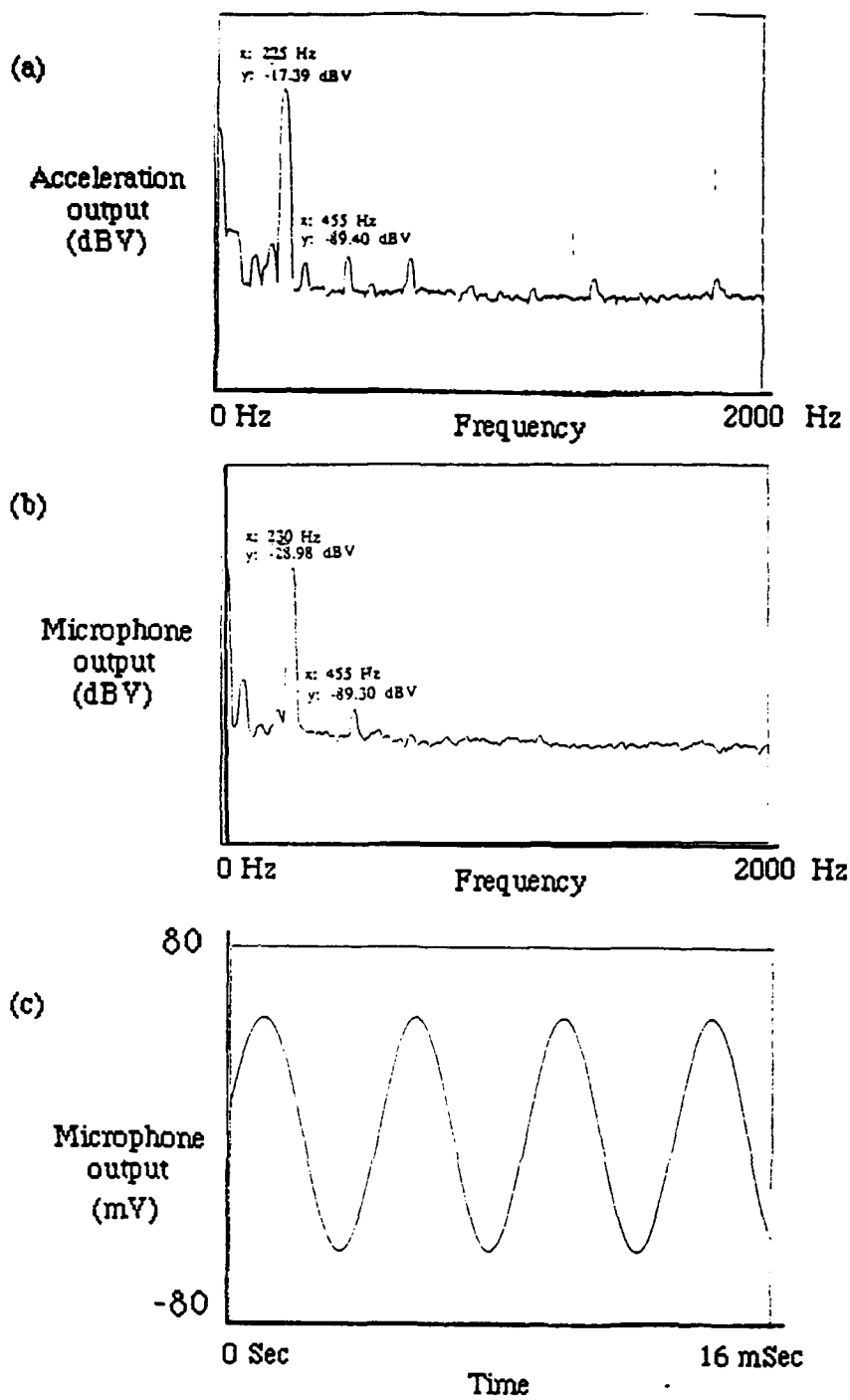


Fig. 17. The spectrum and waveform of the obstructed tube at low Mach number.

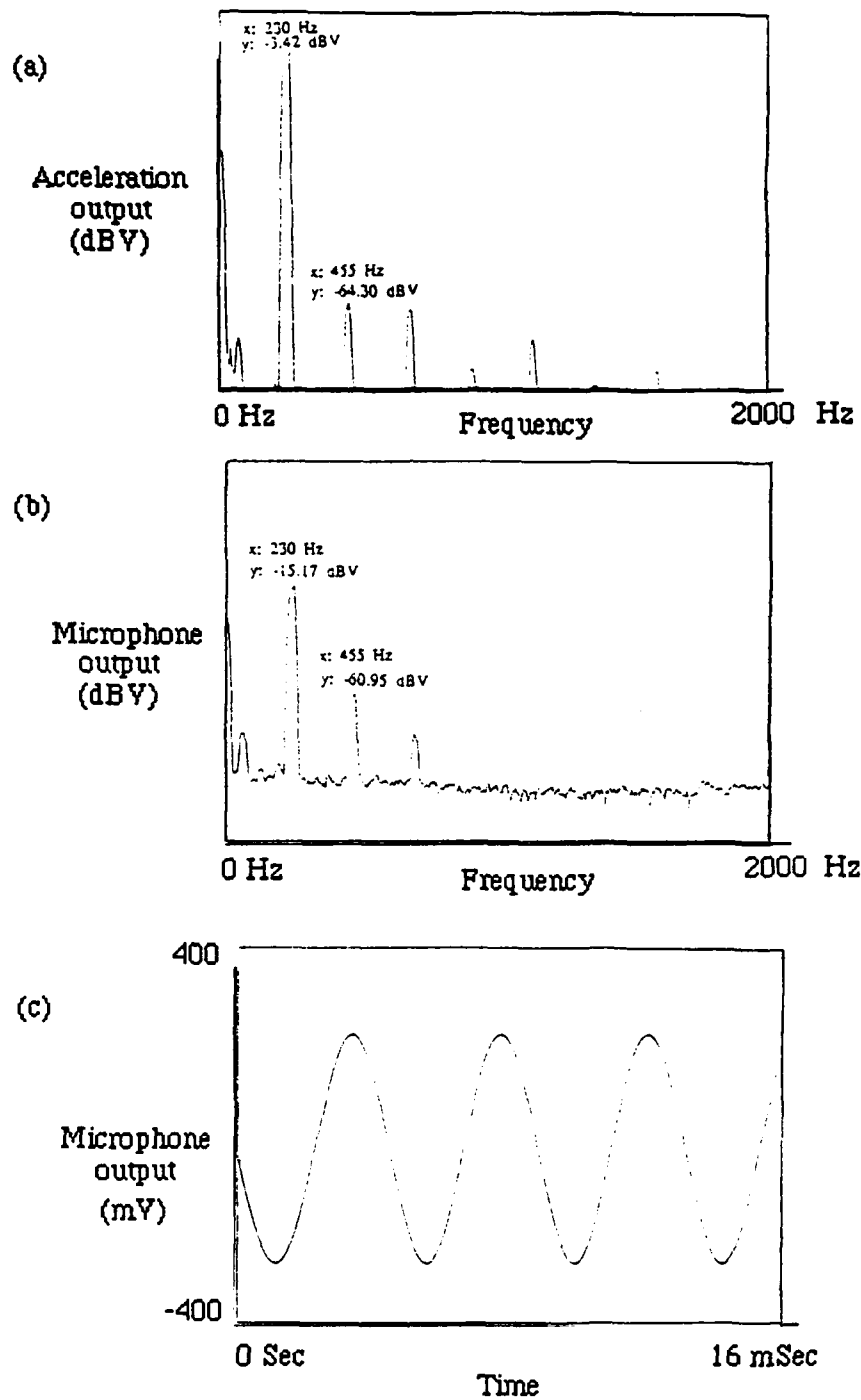


Fig. 18. The spectrum and waveform of the obstructed tube at moderate Mach number.

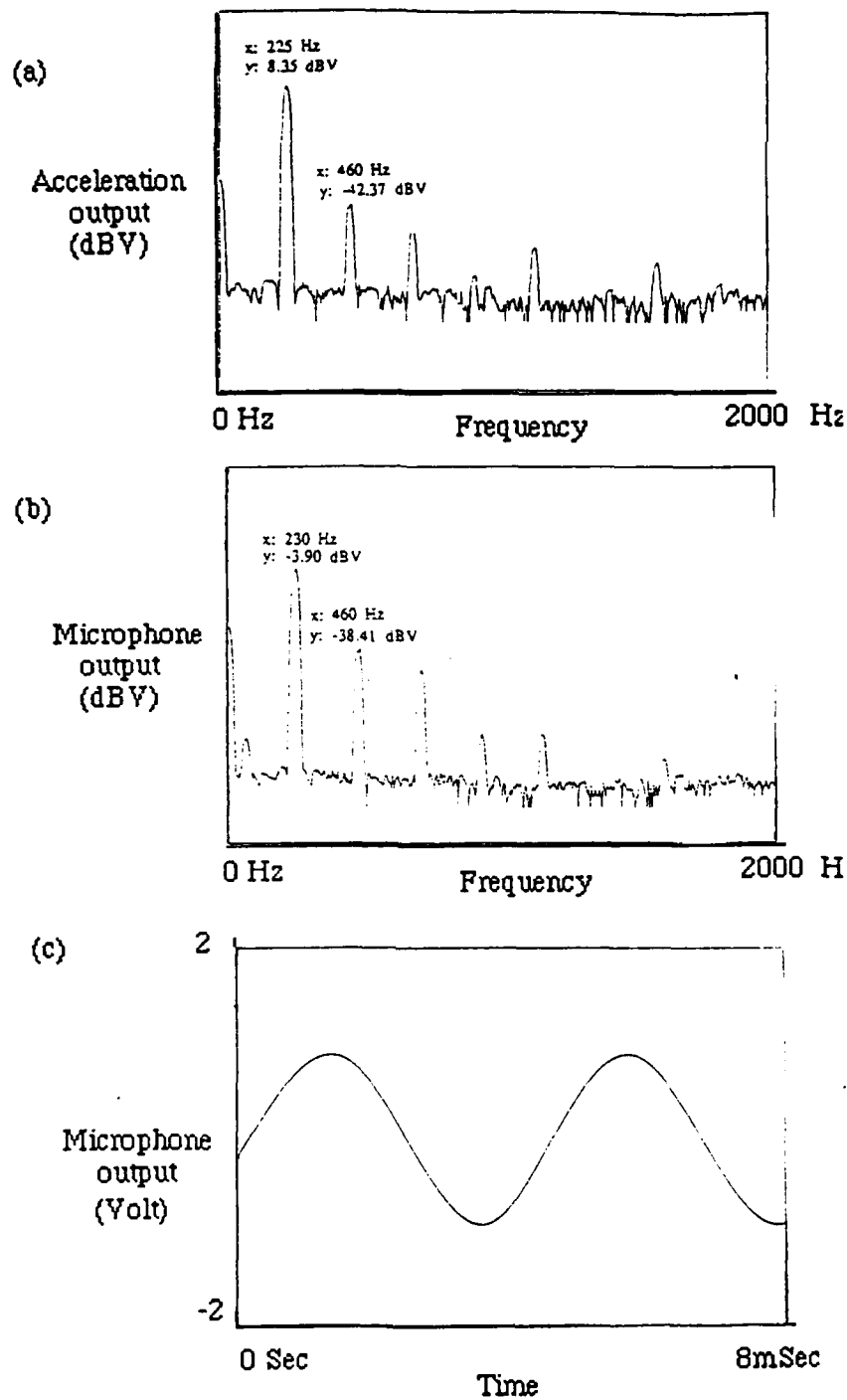


Fig. 19. The spectrum and waveform of the obstructed tube at high Mach number.

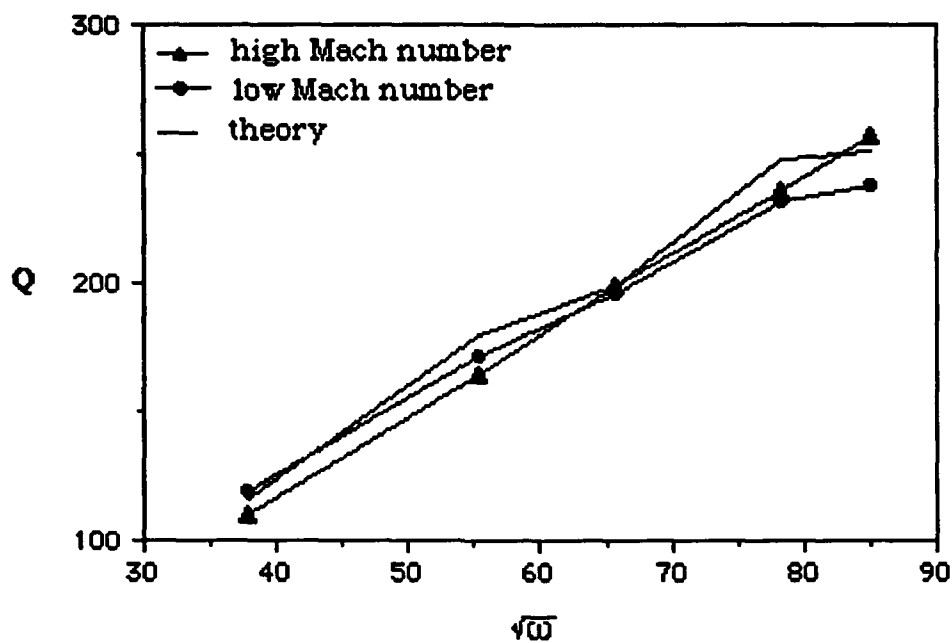


Fig. 20. Experimental Q of the obstructed tube (driven at two different piston Mach number) for the first five modes. Different symbols represent different Mach number: \blacktriangle , Mach number = 4.25×10^{-6} ; \blacktriangle , Mach number = 7.7×10^{-5} . The solid line represents the theoretical Q .

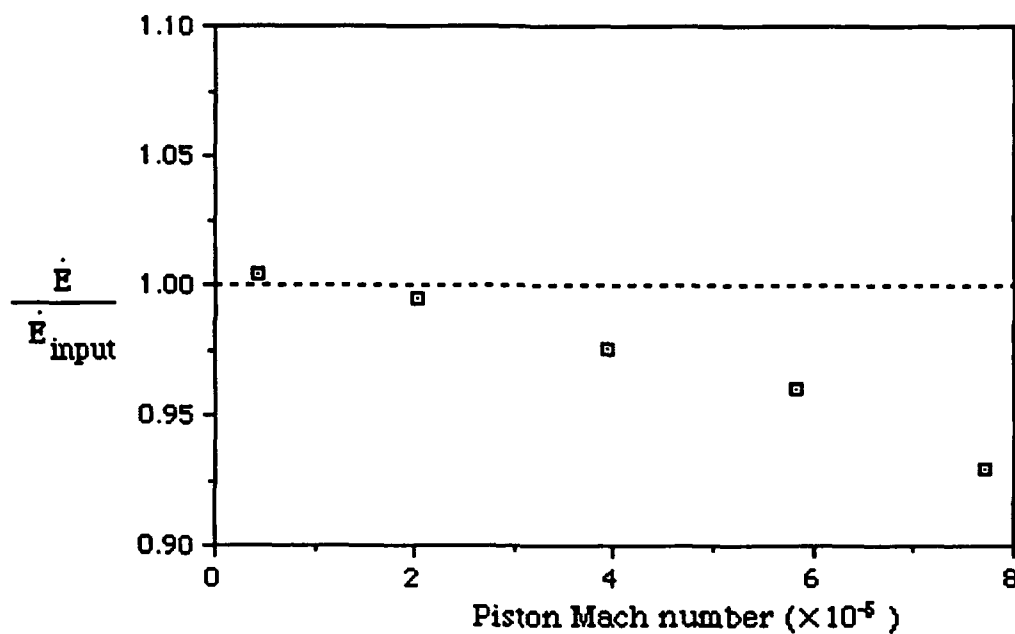
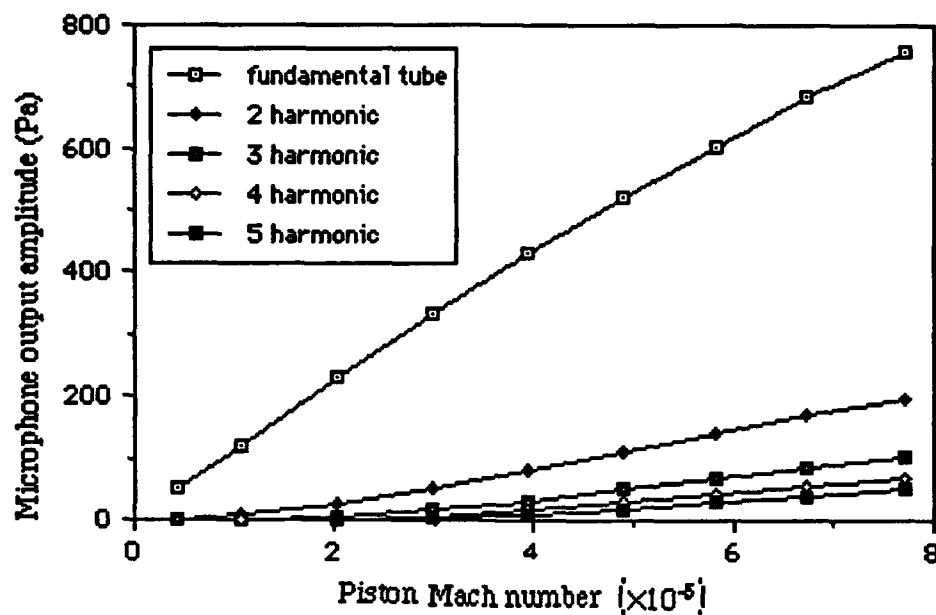
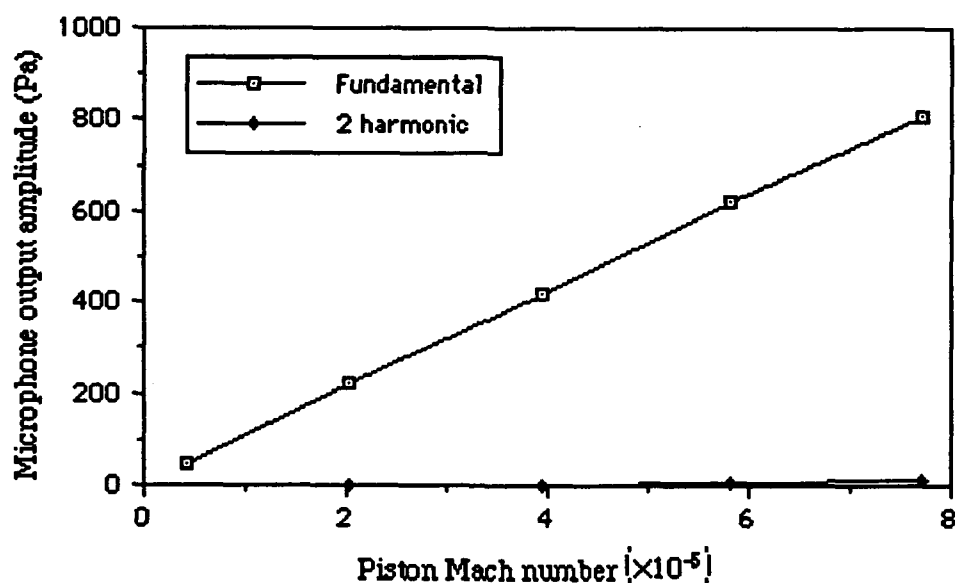


Fig. 21. Ratio of observed $\dot{E} / \dot{E}_{\text{input}}$ versus piston Mach number for the fundamental mode. Points are measured values. The experimental ratio has been compared to the ideal ratio of unity.



(a) Unobstructed tube



(b) Obstructed tube

Fig. 22. Comparison of overall dissipation power by harmonics for unobstructed tube and obstructed tube. The abscissa is the acceleration amplitude in Mach number.

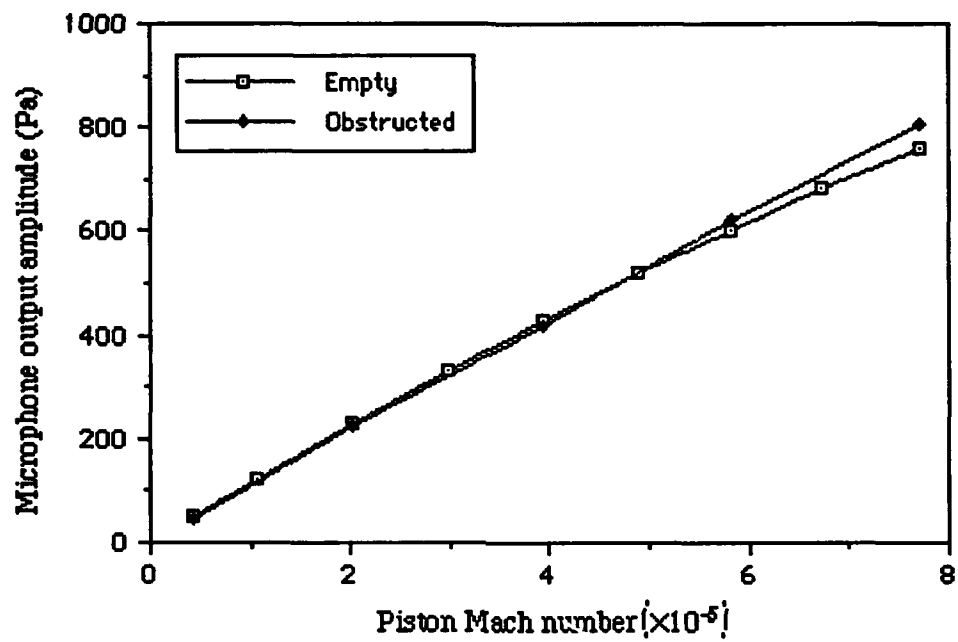


Fig. 23. Comparison of the fundamental component for empty tube and obstructed tube.

V. CONCLUSION

In this study, we used two different tubes: A plain tube (constant cross section) and an obstructed (variable cross section) tube. In these tubes we measure the energy stored in the harmonics generated when the tube was driven at different amplitudes. This was done by calculating the energy dissipated by each harmonic independently based on the observed acoustic pressures. The dissipation of the system as a whole was determined by its quality factor Q . As a result of this research, the following conclusions for were reached.

A. UNOBSTRUCTED TUBE

- When the tube was driven at high amplitudes, harmonics were observed to be large in amplitude and in number.
- Quality factors (Q) for different modes of the tube were measured to be within 5% of the predicted values. Using the measured damping constant, all of the input energy was accounted for as being dissipated by harmonics (including the fundamental) through classical viscous and thermal damping at the tube walls.
- Up to 15% of the energy input into the system was measured to be dissipated by the harmonics.

B. OBSTRUCTED TUBE

- When the tube was made anharmonic by placing a concentric, tubular obstruction in the middle of the tube, the harmonics of the driving frequency were greatly suppressed. In this case, the total energy dissipated by the harmonics was less than 1% of the input energy.
- The ratio of $\dot{E}/\dot{E}_{\text{input}}$ decreases with increasing piston Mach number. The reasons for this decrease are not understood. Possible reasons are excess attenuation due to unavoidable cavities between the tube

and obstruction or turbulence at the boundary of the obstruction. This topic needs further investigation.

- It was successfully demonstrated that nonlinearly-generated harmonics can be suppressed by changing the cross section of the tube near the middle section.

LIST OF REFERENCES

1. Lin, Hsiao-Tseng, "Investigation of a heat driven thermoacoustic prime mover," NPS thesis. Naval Postgraduate School, Monterey, Ca, 66pp.
2. A. A. Atchley, H. E. Bass and T. J. Hofler, "Development of nonlinear waves in a thermoacoustic prime mover," *Frontiers of Nonlinear Acoustics 12th ISNA*, edited M. F. Hamilton and D. T. Blackstock (Elsevier Applied Science, New York, 1990), pp. 603-608.
3. Alan B. Coppins and James V. Sanders, "Finite-amplitude standing waves in rigid-walled tubes," *J. Acoust. Soc. Am.* Vol. 43, No. 3, 516-529 (1968).
4. G. W. Swift, "Thermoacoustic engines," *J. Acoust. Soc. Am.* Vol. 84, 1145-1180 (1988).
5. J. W. S Rayleigh, *The theory of sound* (Dover, 1945), 2nd ed.
6. L. E. Kinsler, A. R. Frey, A. B. Coppins, and J. V. Sanders, *Fundamentals of acoustics* (Wiley, New York, 1982), 3rd ed.

INITIAL DISTRIBUTION LIST

	No. Copies
1. Defense Technical Information Center Cameron Station Alexandria, Virginia 22314-6145	2
2. Library, Code 52 Naval Postgraduate School Monterey, California 93943-5100	2
3. Chairman, Code PH Department of Physics Naval Postgraduate School Monterey, CA 93943	1
3. Chairman, Code PH/ Ay Department of Physics Naval Postgraduate School Monterey, CA 93943	5
4. Prof. Alan B. Coppens, Code PH/Cz Department of Physics Naval Postgraduate School Monterey, CA 93943	1
5. Dr. Felipe Gaitan Department of Physics Naval Postgraduate School Monterey, CA 93943	1
6. LCDR Chen, Chih-Lyeu 4F, 10, Lane 70, Yu-Feng Street, KU-HSAN Kaohsiung, TAIWAN, R. O. C.	3
7. Naval Weather Center P.O. Box 90158 , PA-LI, Taipei county TAIWAN, R. O. C.	3
8. Lieutenant KUO, FENG-MING SMC# 1723 NPS	1

MONTEREY, CA. 93943

- | | |
|--|---|
| 9. DR. CHEN, CHIH-YANG
TAIPEI SUPREME COURT
TAIPEI, TAIWAN, R. O. C. | 1 |
| 10. Captain Lin, Hsiao-Tseng
Department of Vehicle Engineering
Chung Cheng Institute of Technology
Ta-Shih, Tao-Yuan, 33500
Taiwan, R.O.C. | 1 |
| 11. Library of Chinese Naval Academy
P.O. Box 8494 Tso-Ying,
Kaohsiung, Taiwan
Republic of China | 2 |
| 12. Library of Chung-Cheng Institute of Technology
Tashih, Tao-Yuan, Taiwan
Republic of China | 2 |